

# Electron Interferometer Investigation for Coherent Electron Transport in Organic Molecules

Mostafa Moonir Shawrav

June 23, 2010

NANO ELECTRONICS.

**MESA+**

Institute for Nanotechnology

UNIVERSITY OF TWENTE.

Examination Committee Members:

Prof. dr. ir. W.G. van der Wiel	Chairman
Ir. Tian Gang	Daily Supervisor
Dr. ir. M.P. de Jong	Member
Prof. dr. ir. H.J.W.Zandvliet	External Member
Dr. ir. A Brinkman	External Member

The work in this Master thesis has been performed in the NanoElectronics Group of the MESA+ Institute for Nanotechnology and submitted in partial fulfillment of the requirements for the degree Master of Science in Nanotechnology under Faculty of Science and Technology, University of Twente.

Copyright ©2010 by Mostafa Moonir Shawrav

# Abstracts

---

This project aims to investigate the degree of coherence of electron transport through organic molecules. An Aharonov-Bohm ring has been chosen as a probe for coherence transport of the electrons. Three different structures namely hexagonal AB ring, junction with space and line with gap have been designed to observe AB oscillation, increase the resistance of the junction and insert the nanoparticles in different gaps respectively. Electron-beam lithography has been used to write the structure as the device dimension is far below the diffraction limit of light.

A new sample holder has been designed where the voltage probe and current supply are in the same twisted pair. The sample holder is also mounted at the cold finger. All the wirings of the new sample holder have been completed successfully.

Aharonov-Bohm oscillations with reproducible AB period have been observed with the help of sensitive measurement electronics and a cryogenic setup. Subsequently further investigation on the effect of geometry, temperature and the excitation current to the AB oscillation was done. Measured AB period of the oscillation is in agreement with the theoretical value for rings with different dimensions. Also a superconducting behavior due to the contact pads has been observed.

In future, nanoparticle bridging technique can be used to insert monolayer of molecules into the Aharonov-Bohm ring to investigate the effect of the molecule on the coherence.

# List of Abbreviations

---

Aharonov - Bohm	AB
Centimeter	cm
Deionized	DI
Electron Beam	e-beam
Fast Fourier Transform	FFT
Gold	Au
Hertz	Hz
Isopropanol	IPA
Kilo Volt	kV
Micrometer	$\mu\text{m}$
Milli Tesla	mT
Millimeter	mm
Nano Ampere	nA
Nano Volt	nV
Nanometer	nm
Nanoparticles	NPs
Pico Ampere	pA
Revolutions per minutes	rpm
Scanning Electron Microscope	SEM
Self-assembled monolayer	SAM
Silicon Dioxide	SiO <sub>2</sub>
Titanium	Ti

# Table of Contents

---

## Chapter 1: Introduction

1.1	Introduction to Nanoelectronics .....	3
1.2	Motivation of the Experiments .....	3
1.3	Outline of the Report .....	3
1.4	Acknowledgments .....	4

## Chapter 2: Theory and related work

2.1	Aharonov-Bohm effect .....	7
2.2	Phase coherence length .....	9
2.3	Aspect Ratio.....	10
2.4	Nanoparticle Bridging .....	10
2.5	Research Strategy .....	12
2.6	Earlier Works.....	13

## Chapter 3: Sample Layout and Fabrication

3.1	Design.....	16
3.2	Wafer.....	18
3.3	e-beam Lithography .....	18
3.4	Photolithography .....	18
3.5	SEM Images.....	20

## Chapter 4: Measurement Setup

4.1	Heliox VL.....	24
4.1.1	Operating Principle of Heliox VL.....	24
4.1.2	Sample Holder and Wiring .....	25
4.2	Measurement Electronics .....	27
4.2.1	Lock-in SR830.....	28
4.3	Effective Electron Temperature .....	29
4.4	Measurement Diagram.....	30

## Chapter 5: Results and Discussion

5.1	Resistance Measurements .....	33
5.2	AB Oscillations.....	33
5.3	Temperature dependence of AB oscillations .....	38
5.4	Excitation Current Dependence of AB oscillations .....	40
5.5	Behavior near zero magnetic field.....	43
5.5.1	AB oscillations for gold wire bonded ring .....	45
5.5.2	Behavior near Zero Field for gold bonded ring (ring H5) .....	47

## **Chapter 6: Conclusions and Recommendations**

6.1	Conclusions.....	51
6.2	Recommendations .....	52

### **Appendices**

Appendix 1	Mask Layout for contact pads .....	57
Appendix 2	Connection Diagram .....	58
Appendix 3	Calculation of AB Period of a ring.....	60
Appendix 4	Measurement parameters for different rings.....	62

# Chapter 1: Introduction

---



## 1.1 Introduction to Nanoelectronics

Nanoelectronics covers the study of the electronic and magnetic properties of systems with critical dimensions in the range of sub  $\sim 100$  nm. Generally all the electronic processes in nature occur in molecular structures. Molecular electronics is the branch of nanoelectronics that deals with the application of molecular building blocks for fabrication of both active and passive electronic components. As there are several advantages of molecular electronics; like low fabrication cost, self assembly and recognition etc; it becomes more popular day by day.

## 1.2 Motivation of the Experiments

According to Moore's law, the number of transistors on a microprocessor continues to double in every 18 months [1]. In the year 2030, circuits of a microprocessor will be measured on an atomic scale.

As it is a relatively new concept, molecular electronics has not been completely explored yet. The main purpose of this project is to explore the coherency of electron transport in organic systems. Molecules internal parameters like chemical bonding, length, composition or external parameters like magnetic field may have effects on the coherency of the electron transport. A transport can be said as 'coherent transport' if electron preserved its phase memory during traveling around a ring like geometry.

One of the possible applications of this project could be quantum computation. In quantum computers, it is essential to observe the phase information of the system. Coherency is needed to look at the phase information. Moreover, introduction of the organic components to the quantum circuit also gives possible advantages in fabrication. So a comprehensive study is needed to see whether the electron transport is coherent or not. Also if it is coherent, factors affecting the coherency need to be investigated.

## 1.3 Outline of the Report

*Chapter 1* is divided into four parts. The first section presents a general introduction to nanoelectronics, molecular electronics and the Aharonov-Bohm (AB) effect. The second section gives the motivation of the experiments, followed by the outline of the report and the acknowledgements.

*Chapter 2* reviews the theoretical background of the work presented in this thesis. In the first sections, some theory is presented followed by a discussion of earlier works related to the topic of this thesis. Then the research strategy is described, which links theory and the experimental work.

*Chapter 3* explores the sample layout with the design and explanation, including a detailed description of the sample fabrication procedure.

*Chapter 4* describes the measurement setup. The operating principle of the Heliox VL and measurement are explained.

*Chapter 5* contextualizes all the measurement results of the experiments. Also discussions of the results are presented in this chapter.

*Chapter 6* summarizes the achievements of the projects. Based on the results, recommendation has made for the future project.

## 1.4 Acknowledgments

It is a pleasure for me to thank the people who made this thesis possible.

First of all, I would like to express my appreciation to Prof.dr.ir. Wilfred Van der Wiel and Tian Gang. I learned a lot from both of you. Wilfred, Thank you very much for giving me the opportunity to be part of the NanoElectronics Research group. It has been an honor for me to work with you. Tian, I am really grateful to you for all kinds of help, you are the best supervisor I've seen in my life.

I would like to gratefully acknowledge the help from other committee members – Prof.dr.ir. H.J.W.Zandvliet, Dr.ir. A Brinkman, Dr.ir. Michel de Jong. Thank you all for the useful discussion during the mid evaluation of my Master thesis and be a part of my committee.

My gratitude also goes to Mr. Yoshida-San from the Group of Prof.Seigo Tarucha, University of Tokyo and Mrs. Anja van Langen from Delft University of Technology for EB writing of our samples. I appreciate the time and effort they put for making such a fantastic sample. I'm also grateful to our great Technician Ing. Johnny Sanderink for the wonderful SEM images.

I am privileged to be a part of the Nanoelectronics Research group. I would like to thank all the member of the group for their cooperation – our Secretary Carolien and Joyce, Ina Rianasari (for being the supervisor of my research project on nanoparticle insertion), Bernadus Zijlstra (for helping me to get used with Clewin software), Thijs, Martin, Wouter, Ivan, Johnny W, Jean, Yunjae, Lan, Serkan, Eerkes, Saroj and Sandeep. Thanks to the the student member of our group for a nice working environment – Michel, Peter, Maarten, Koert and Lucky. I would also like to thank Harry Steffens for providing the helium in time and other member from T2 specially Sander Wessel and Erik Krooshoop.

I would like to thank the program director of master nanotechnology Dr. Jaap Flokstra ( Thanks for listening our views about the program), Dr. Martin Bennik ( I really like that you always had some time for the students – may be at the middle of the oral examination or after a conference talk; even between the concerts at Switzerland) and Rik Akse (for being a real guardian of an international student) and I am also grateful to the fellow Master Nanotechnology students for all their help during last 2 years specially Maike Baltussen, Verena Stimberg, Bob Lansdorp and Gao An.

I am grateful to the other Bangladeshi students at Enschede for giving me a homely feeling - Ashique, Reza, Atik, Rabbu, Rezwan and Dhrubo. Very special thanks to Mr. Sirajul Kabir for you inspiration about my career. I am also thankful to all of my friends and well wishers for supporting me throughout my career.

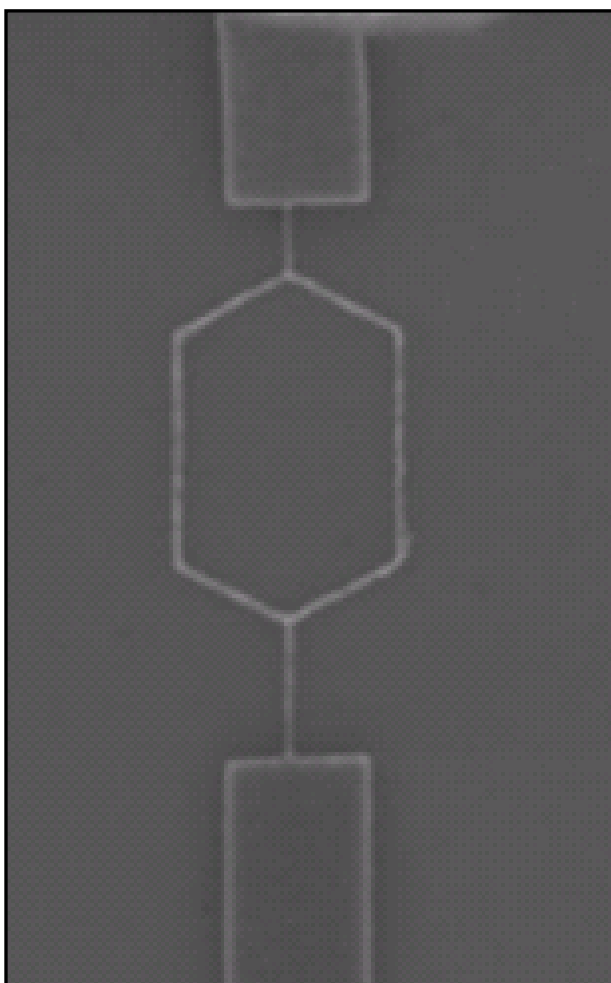
A special thanks goes to my wife- Anupoma, thank you very much for the unconditional support through all this long process.

My final words go to the most important persons of my life – my parents and brother. I'm really grateful to you for all the support you provided me throughout the whole life. Today I'm here only because of you.

Thank you all.

## Chapter 2: Theory and related work

---



## 2.1 Aharonov-Bohm effect

Generally from classical mechanics it can be distinguished that the motion of a charged particle is not affected by the presence of a magnetic field in regions from which the particle is excluded [2]. In Figure 2.1, where S is the source, B is the magnetic field and D is the detector and white arrows define the electron path, it is illustrated that the motion of the particles which are emitted by Source S will not be affected by B. The reason behind is that it is not possible for the particles to enter the region where the magnetic field is present.

However, a significant phase shift in the interference pattern can be visible for a quantum charged particle. This phase shift can be detected by the detector D. The main reason behind this behavior is that although it is true that there is no magnetic field in the particular region that can be accessed by the particle, an associated non-zero vector potential exists. As can be seen from Figure 2.1, there are two alternative paths “a” and “b”; the phase shift depends on the flux enclosed by the two paths. There is no classical magnetic force present on the particles. But quantum mechanically it is possible to change the properties of the electron. This effect is known as the Aharonov-Bohm (AB) effect. It illustrates that the electromagnetic potentials are the fundamental quantities in quantum mechanics.

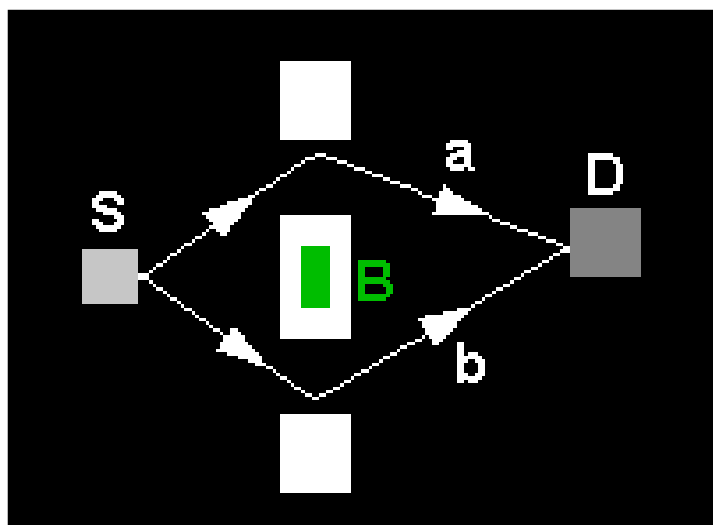


Figure 2.1: Electron trajectories “a” and “b” between source, S, and drain, D, enclosing a magnetic field B. Reproduced from Ref. [2].

When the magnetic flux threading the loop is increased, the electrical resistance oscillates periodically with a period of  $h/e$ , i.e. the normal-metal flux quantum ( $h$  is Planck’s constant and  $e$  the charge of the electron). The electrical resistance fluctuates randomly as a function of magnetic flux in single wires due to universal conductance fluctuations (UCF).

A practical device to measure such an effect is shown in Figure 2.2 [3]. Electrons having two different phases for transport through the upper and

the lower arm are denoted by  $\phi_1$  and  $\phi_2$ . Electron waves travelling through the two parallel paths obtain two different phases. Thus, the resulting electron wave (when two partial electron waves again meet) can be described as the superposition of these two waves. The amplitude of the resulting electron wave depends on both the amplitude and the phase of those two partial electron waves.

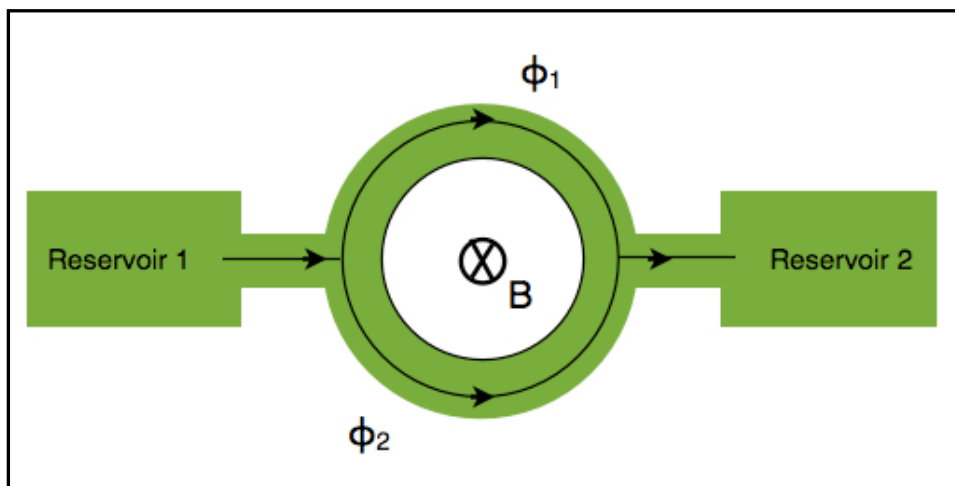


Figure 2.2: Schematic representation of an AB ring.

The relative phase difference ( $\Delta\phi$ ) of an electron due to the magnetic vector potential by traveling along the path L can be calculated in the following way,

$$\begin{aligned}\Delta\phi &= \phi_1 - \phi_2 \\ &= 2\pi \left(\frac{e}{h}\right) \oint \vec{A} \cdot d\vec{l} \\ &= 2\pi \left(\frac{e}{h}\right) \oiint (\vec{\nabla} \times \vec{A}) \cdot d\vec{S}\end{aligned}$$

$$\text{As, } \vec{\nabla} \times \vec{A} = \vec{B} \text{ and } \oiint (\vec{B} \cdot d\vec{S}) = \phi.$$

$$\Delta\phi = 2\pi \left(\frac{e}{h}\right) BS_{\text{in}} = 2\pi \left(\frac{\phi}{\phi_0}\right) \quad (1)$$

Here,  $B$  is magnetic field,  $A$  is the magnetic vector potential,  $S_{\text{in}}$  the enclosed area of the ring,  $\phi$  is the magnetic flux through the enclosed area,  $\phi_0 = h/e$  the flux quantum.,  $\phi_1$  is the phase shift of the electron traversing from upper arm  $\phi_2$  is the phase shift of the electron traversing from bottom arm.

The relative phase difference of the two waves changes when the magnetic field changes. This phase difference could be zero or a multiple of  $2\pi$  at a particular magnetic field. At this field, two partial waves interfere constructively which represent the maximum amplitude of the total wave. The resistance is minimum in that particular field. Similarly, at certain fields the relative phase difference could be  $\pi$ . At this point destructive interference

occurs and the maximum resistance can be obtained from the ring. When the magnetic field is swept continuously, a resistance oscillation is observed. One period can be calculated as

$$\Delta B = \frac{\phi_0}{S} = \frac{h}{eS} \quad (2)$$

Several studies found that generally the amplitude of  $h/e$  oscillations is about 0.1% of the resistance at zero field at low temperature (around 100 mK)[4].

This phenomenon was first predicted by Yakir Aharonov and David Joseph Bohm [5]. That is why it is called Aharonov-Bohm effect. The first experimental verification was on a single diffusive metal rings by Webb *et al.* in 1985 [4].

Universal conductance fluctuations (UCF) is a phenomenon which occurs due to quantum physics during the electrical transport experiments of the mesoscopic objects. This variation happened because of the inhomogeneous scattering sites. Coherence effect is the reason of these fluctuations. This is also related to the magnetic field. This depends on the device geometry. Origin of UCF is the same as of AB oscillations. As the geometry of the interference paths is not well defined in the case of UCF, one gets *fluctuations* instead of oscillations. Mesoscopic theory predicts that the amplitude of both UCF and AB are on the order of  $e^2/h$ .

According to the UCF theory [6], the conductance of any (semi-)conducting sample will be fluctuating as a function of chemical potential or magnetic field on the order of  $e^2/h$ , independent of sample size and degree of disorder as long as the coherency is maintained. This theory indicates that coherency of the sample contributes to the fluctuations.

AB rings are chosen for this study, as phase information of the electrons can be probed by these rings. The presence of molecular layer in an AB ring could change the phase information of the electron passing through the arm. The characterization of the coherency of electron transport through organic molecules can be achieved by inserting a molecular monolayer in the Aharonov-Bohm interferometer ring.

## 2.2 Phase coherence length

The phase coherence length is defined as the distance between inelastic collisions or other phase randomizing events. Electrons “remember” their phase information over a certain distance, this distance is called the phase coherence length. It is denoted by  $l\phi$ . The AB effect in ring (Length L) can be observed only if electrons can keep their phase information when traveling along that ring. This will only happen if  $L/2$  is less than  $l\phi$ . So the phase coherence length at the measurement temperature needs to be greater than the length of the electron path.

The phase coherence length also depends on temperature. If the temperature is increased, the phase coherence length will become shorter as expected [7]. In this experiment, gold is used to fabricate the device, which has a phase coherence length of  $\sim 1\mu\text{m}$  at 250 mK [8].

### 2.3 Aspect Ratio

The aspect ratio of a ring is defined as the ratio between the area enclosed by the ring and the area of the arms. A general formula of the aspect ratio with a schematic diagram of a ring is given below:

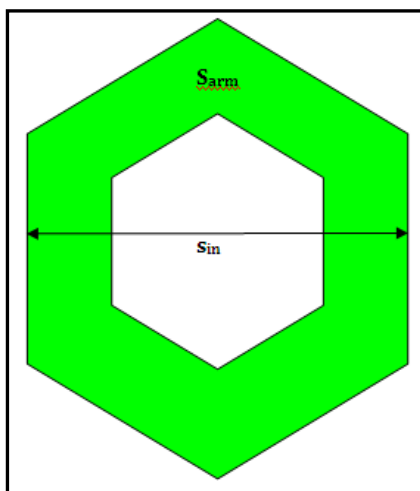


Figure 2.3: Schematic diagram of a ring.

$$\text{Aspect Ratio} = \frac{S_{in}}{S_{arm}}$$

Usually AB phase is defined by the enclosed area of the ring ( $S_{in}$ ) where as UCF is correlated with the area of the arms ( $S_{arm}$ ). If aspect ratio is low, the period of AB oscillations and UCF are on the same order. So AB oscillation can't be observed.

On the other hand, if aspect ratio is high, it is possible to separate the AB oscillations from the UCF. So to observe the AB oscillation, aspect ratio of the ring should be large enough (at least greater than 1).

As unsymmetrical ring is used for this project, it is not possible to give any general formula for the aspect ratio. However, aspect ratio of the rings is calculated from the design file and is presented in the Chapter 5 of this thesis.

### 2.4 Nanoparticle Bridging

“NP bridging” is a way to insert molecules in the electronic circuit, the schematic of this technique is given in Figure 2.4.

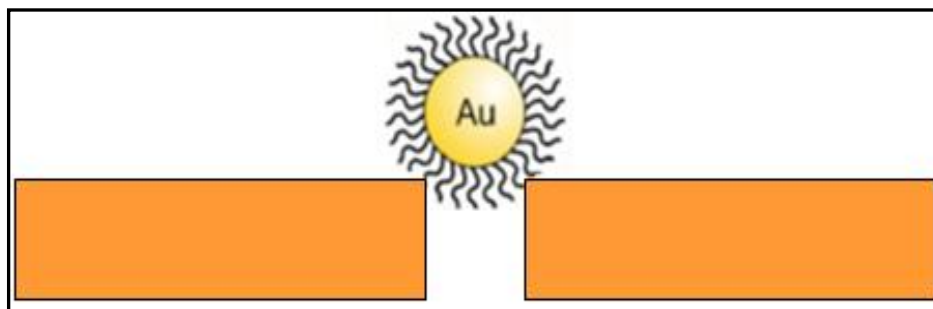


Figure 2.4: Schematic diagram of the NPs Bridging.

One of the notable applications of this technique has published by Almani *et al* [9]. First, a self-assembled monolayer was formed of the molecule of interest on a pair of electrodes. After that the gap between two electrodes were bridged by metallic NPs using an alternating electric field. NPs face a dielectrophoretic force due to the presence of ac field; which pulls them in the direction of maximum field strength between the gap. Also it is possible to use direct current field for this procedure. But it was found that alternating field provided the expected result.

Both e-beam and typical photolithography was used to fabricate metallic electrodes. Au electrodes were made with gaps ranging from 40nm to 100nm. Results of the experiments are shown in Figure 2.5[9].

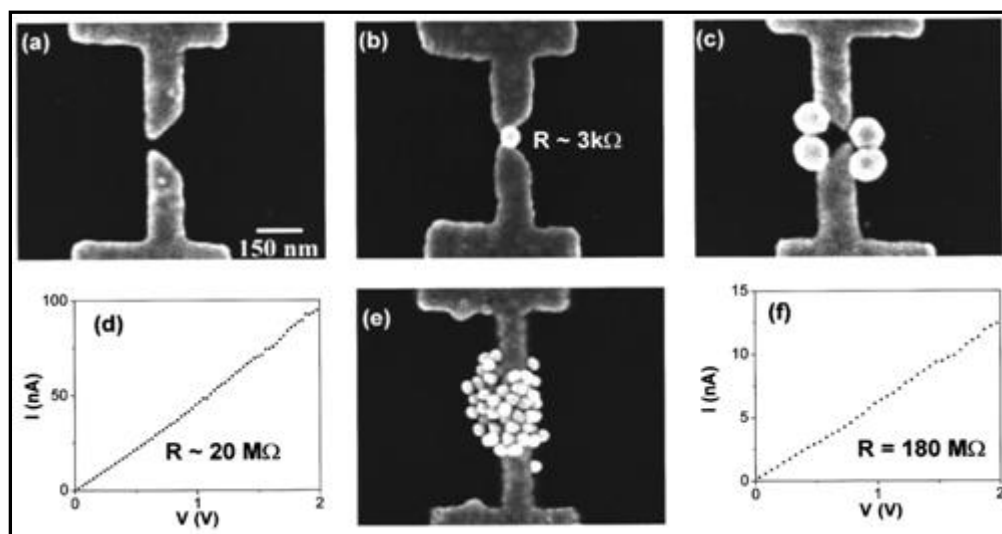


Figure 2.5: Characterization of Au-electrode NPs contact. a) SEM image of fabricated electrodes b) SEM image of 80nm Au Nps in 60nm gap c) SEM image of 120nm Au Nps in 40nm gap d) I-V characteristics for c); e) SEM image of 120nm Au Nps in 40nm gap f) I-V characteristics for e).

From this study, it is found that during NP insertion particle and gap size need to have a good match. For the purpose of this project, it is good to have a larger particle size than the gap to reach a lower resistance. (Figure 2.5b, Figure 2.5c). Moreover, in one gap only one particle is desired; having more than one particle could result in a high resistance. For example, in Figure 2.5e,

multiple numbers of NPs in a gap causes the high resistance. On the other hand, four particles in a gap give much lower resistance.

## 2.5 Research Strategy

An AB interferometer is chosen as a probe for coherent electron transport. There are two parts of this project – Measuring AB oscillation and inserting NPs in the gap. The desired layout of the sample after NP bridging is shown in Figure 2.6.

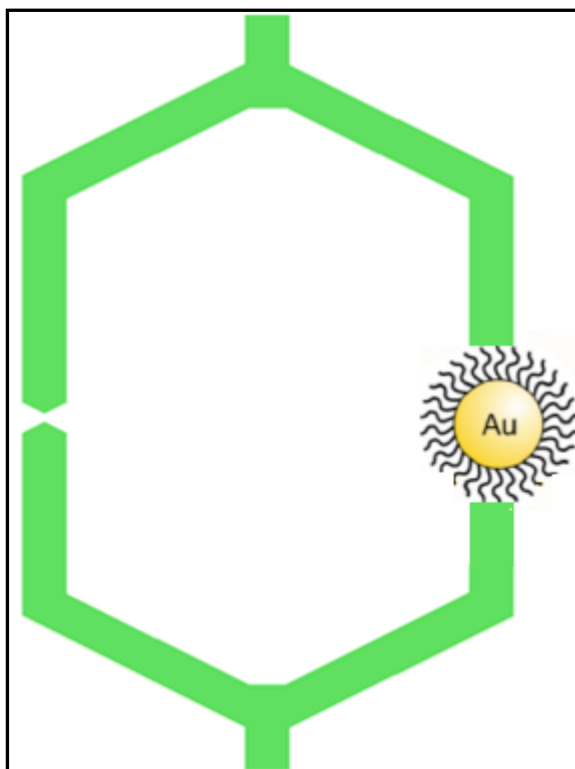


Figure 2.6: Schematic diagram of the desired look of AB ring. Gap is closed by an Au NP.

A molecular monolayer is inserted into the electron path by NP bridging. To insert the NPs in an AB interferometer, a gap structure is defined in one arm of the AB ring. The low resistance on the other arm will cause unbalance between two conduction paths. That is why special junction structure with some spaces is made in the other arm of the AB ring. So at first, three types of structures are defined with e-beam lithography namely – Ring, Junction with gap and Line with gap.

Then photolithography will be used to define the contact pads. After successful completion of the fabrication procedure, the sample will be assessed by SEM. The detailed device fabrication procedure is explained in Chapter 3.

A cryogenic setup and sensitive measurement electronics are essential to observe the AB oscillations. If it is possible to observe AB oscillations in the

complete rings, then reproducibility of the oscillations need to be checked. Also it is important to measure the effect of temperature and excitation current.

Then NPs insertion will be used to close the nanogaps. During NPs selection, the size of the NPs needs to be chosen carefully. SEM will be used to check the NPs insertion. Afterwards some measurement will be taken of the rings where the gap is closed by the NPs.

## 2.6 Earlier Works

One related work, performed by NanoElectronics research group of University of Twente in 2009, had been reported in this field [3]. Nanoscale metallic (Ti Au) rings were fabricated on top of an insulating substrate ( $\text{SiO}_2$ ). The ring included a sub 100nm gap. Main objective was to close the gap with NPs bridging in a way that a molecular monolayer was inserted in the conduction path (Figure 2.7).

Two kinds of rings were used in that experiment – circular and hexagonal. In circular rings, there were some problems that occurred during the fabrication process. One of them was due to an inappropriate metal lift-off process; metal could be observed even inside the rings. Moreover, during E-beam lithography, due to over-exposure, the aspect ratio of the rings became lower than 1, which makes it difficult to observe Aharonov-Bohm oscillations.

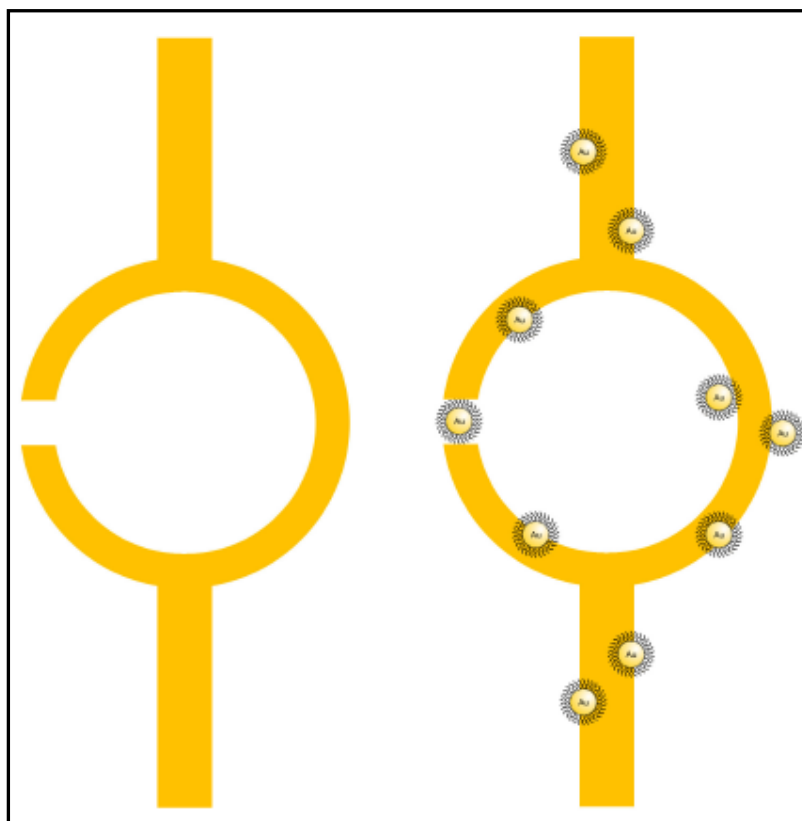


Figure 2.7: Schematic diagram of a) a metallic ring b) desired look of the gap and rings after NPs bridging [3].

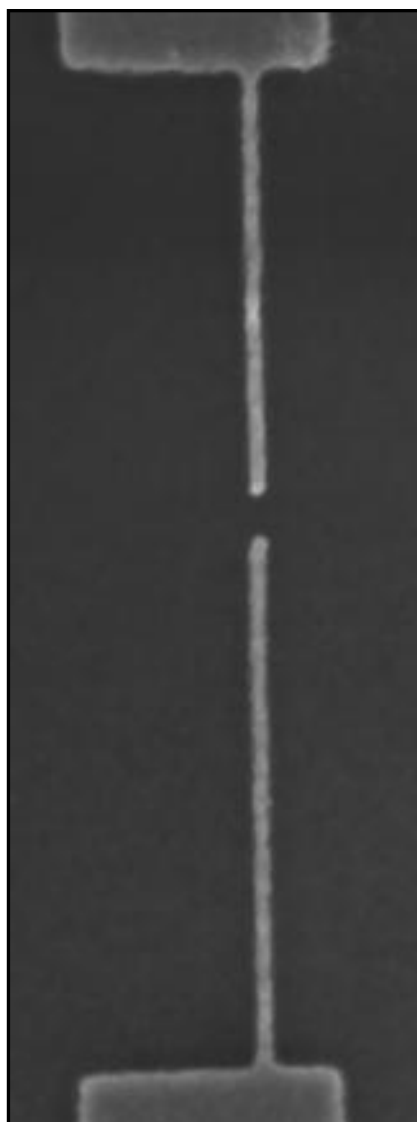
In case of hexagonal samples, the resistance of the junction was not high enough for insertion of the NPs. Resistance of the rings with junction is in the order of 2 k ohms. However, since the electrons tunnel through the molecules to the metallic From the previous study described in the section 2.4, NPs and the tunneling resistance is about 20 MOhm, so the resistance of the junctions should be in the order of 20 MOhm.

Finally it was not possible to achieve the ultimate goal mainly due to two reasons – low resistance at junction and using single wire during measurement setup (this part has described detail in Chapter 4).

In this project, the findings of the previous study have taken into consideration.

## Chapter 3: Sample Layout and Fabrication

---



The nanoscale ring patterns are defined by e-beam lithography followed by metallization and a metal lift-off process. Then photolithography, and a second metallization and metal lift-off have been applied to make the larger contact pads. These contact pads are used for wire bonding. When the fabrication procedure has been completed, the samples are assessed by SEM.

### 3.1 Design

As explained in earlier chapter, during the design phase, couples of things need to be considered. Among them, phase coherence length and aspect ratio are the most important ones. In general, phase coherence length should be greater than the path length of electron and aspect ratio of the ring must be larger than one. There are mainly three types of structures in the sample – Hexagonal AB Ring marked as green, junction with space marked as red and line with gap marked as black in the detail design map of the e-beam structure in Table 3.1. Each of these structures has different objective. Gap size zero corresponds to the fact that there is no gap in the structure.

Table 3.1: Design map of the e-beam structure of AB rings.

Ring	1-4	5-8	9-12	13-16	17-20	21-24	Type of structure	Dimension (nm)
A	0	0	1	1	2	2	Junction with space	space size
B	300	300	300	300	300	300	Ring	Width of the ring
C	3	3	4	4	5	5	Junction with space	space size
D	400	400	400	400	400	400	Ring	Width of the ring
E	6	6	7	7	8	8	Junction with space	space size
F	500	500	500	500	500	500	Ring	Width of the ring
G	9	9	10	10	12	12	Junction with space	space size
H	600	600	600	600	600	600	Ring	Width of the ring
I	0	2	4	6	8	10	Junction with space	space size
J	700	700	700	700	700	700	Ring	Width of the ring
K	80	80	70	70	60	60	Line with gap	gap size
L	800	800	800	800	800	800	Ring	Width of the ring
M	50	50	40	40	30	30	Line with gap	gap size
N	900	900	900	900	900	900	Ring	Width of the ring
O	20	20	10	10	0	0	Line with gap	gap size
P	1000	1000	1000	1000	1000	1000	Ring	Width of the ring
Q	0	0	20	40	60	80	Line with gap	gap size

As mentioned earlier, hexagonal pattern has chosen for the ring design. Width of the ring varied from 300 nm to 600 nm. The arm width of the ring is 40 nm. Clewin design drawing of a 600nm width ring have shown in the Figure 3.1.

To increase the resistance of the junction, very small spaces inside the junction have initiated. The space size gap size varied from 0 to 12 nm. It is used to fabrication a constriction in the arm. A corresponding schematic diagram and the Clewin design drawing have shown in Figure 3.2.

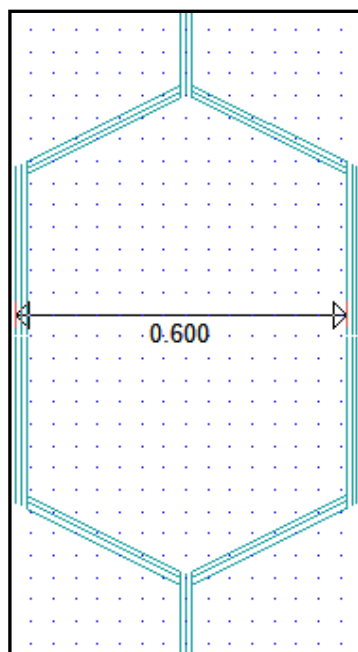


Figure 3.1: Clewin Design for the hexagonal ring. Width of this particular ring is 600nm.

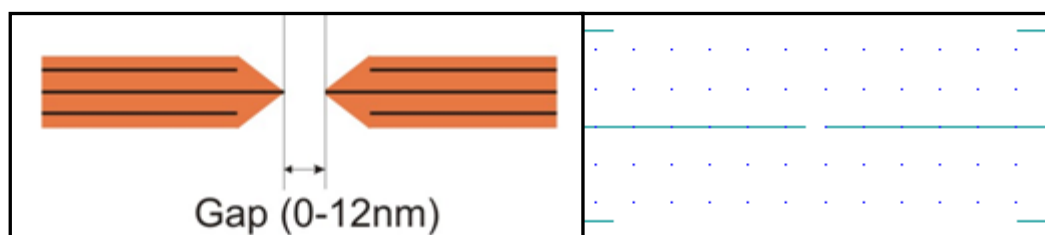


Figure 3.2: Schematic diagram of the junction with gap structure (left side) and Clewin design for the same structure (right side). Particular gap size is 12nm (right side).

As reliable gap sizes are needed for NPs insertion, lines with gap structures are introduced. The gap sizes are varied between 0 to 80nm while the width of the line is 40nm. Size of the gap varied to find the optimal gap size during NPs insertion. A schematic diagram and the Clewin design drawing has shown in Figure 3.3 can estimate which size would be best for insertion.

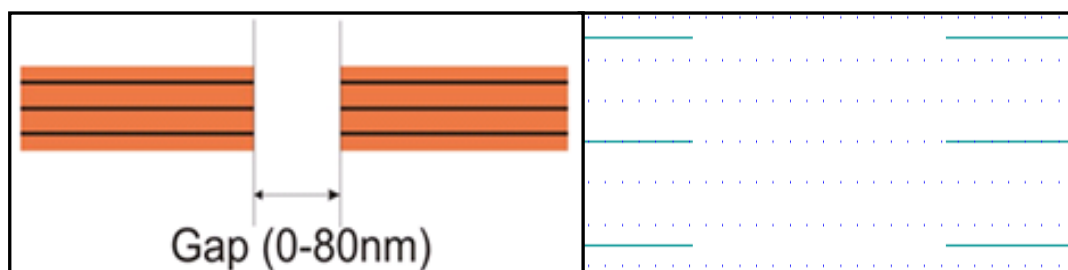


Figure 3.3: Schematic Diagram of the line with gap structure (left side) and Clewin design drawing for the same structure (right side), Particular gap size is 60nm (right side).

### 3.2 Wafer

Samples are prepared on a standard p-type silicon wafer which has <100> orientation. Thickness of the silicon wafer is 545  $\mu\text{m}$ . Then a layer of  $\text{SiO}_2$  was thermally grown on top of the wafer. The thickness of the  $\text{SiO}_2$  layer was 40 nm. As the rings are made with Ti/Au, this  $\text{SiO}_2$  layer works as an insulating layer. The substrate is 10mm x 10mm in size due to the limitation of the e-beam and constrain of the Heliox sample holder.

### 3.3 e-beam Lithography

It's known that the diffraction limit of light is around 200 nm. In this design, the size of the ring pattern is far below the diffraction limit of light. So e-beam lithography is essential to make this type of structure. It is possible to make sub 100nm structure by this type of lithography. An e-beam lithography process has explained in the Figure 3.4.

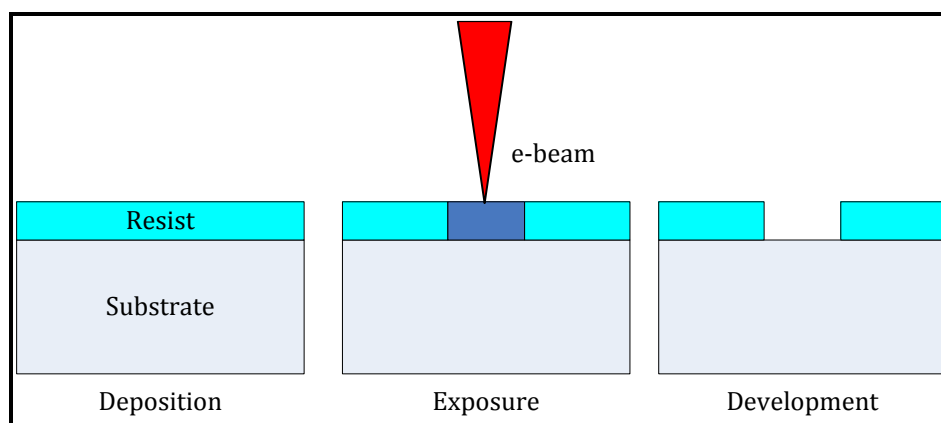


Figure 3.4: Electron Beam lithography Process.

During a typical e-beam lithography process, first a layer of e-beam resist is spun coated onto a substrate. Then a computer controlled electron beam is scanned across the surface and “writes” the required pattern. Then exposed areas are dissolved during developing. Afterward, the pattern is transferred into another material (in this project, this material is gold) by using metal lift off process. Finally, acetone is used to remove the unexposed resist. The metal layer consists of a thin 10nm Ti adhesion layer and 40 nm Au. Dwell time was 1.9microseconds. The e-beam lithography process of the samples was completed by Mr. Yoshida at Prof. Seigo Tarucha’s Group at the University of Tokyo.

### 3.4 Photolithography

Nowadays optical lithography or photolithography is the most universal approach in micro fabrication. This is the process of transferring a pattern on a mask to the surface of a silicon wafer. The contact pads for the sample were

fabricated using typical photolithography. The mask layout for the contact pads can be found in Appendix 1.

Before starting optical lithography procedure, first special cleaning steps were applied to remove the photoresist protection layer. The sample was dipped in the acetone and stirred for 1 hour, subsequently same process followed for IPA for 1 more hour. Then the sample was rinsed with DI water for 1min and spin drying step had performed to dry the sample.

Afterwards, ODP 907/17 positive photoresist was spun using recipe 10 at the spin coater at (500rpm 5sec then 4000rpm for 20 seconds) on the 10mm by 10 mm sample which resulted in a photoresist layer with a thickness of  $1.7\ \mu\text{m}$ . The sample was baked on a hot plate for 1 minute at  $95^{\circ}\text{C}$ . Then alignment of the mask for the contact pads was done followed by 5 seconds exposure. This process must be done very carefully, if there is a problem in the alignment, the e-beam pattern could be totally misaligned with the contact pads. Before developing, the sample was baked at a contact hot plate at  $120^{\circ}\text{C}$  for 1 minute. Then the sample was developed for 1 minute. Finally, the alignment of the optical pattern and the e-beam structure was checked with the optical microscope. Result of the sample after developing can be obtained from Figure 3.5.

It can be observed from Figure 3.5 that AB rings are almost at the middle of the contact pads which means the mask alignment was done perfectly. If anything goes wrong at the lithography step, the whole procured need to be performed again, starting from the cleaning step.

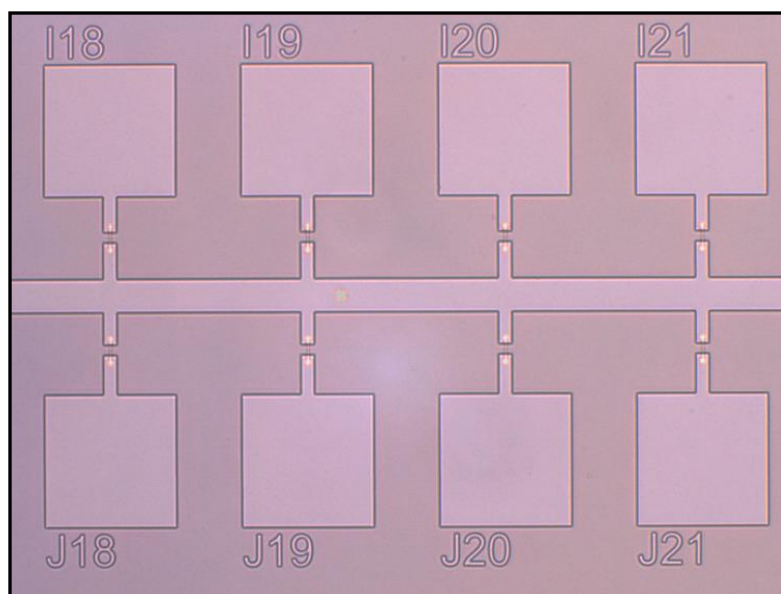


Figure 3.5: Result of optical lithography of part of the line I and J (after developing). Part of the connecting horizontal line can be seen as common contact and the contact pads of the ring. Each ring has  $200 * 200\ \mu\text{m}$  contact pad which is connected to the horizontal line.

Then a metallic thin film was deposited by e-beam evaporation. A layer of 100nm titanium and 500nm gold was deposited, followed by a standard metal

lift off process. In this process, the sample was dipped in the acetone overnight and then cleaned with acetone, IPA and DI water and made it dry using spin drying technique.

This total photolithography procedure has performed in the MESA+ clean room. The result of the deposition can be found in Figure 3.6.

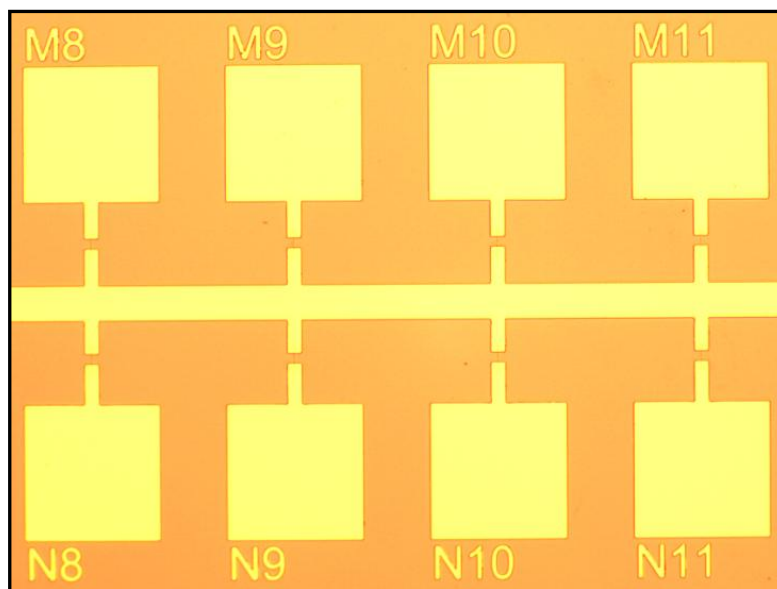


Figure 3.6: Result of the optical lithography (after metal lift off). Part of the line M and N.

### 3.5 SEM Images

After successful completion of the photolithography procedure, the samples were inspected by SEM situated at MESA+ Cleanroom with help of Ing. Johnny Sanderink. All the SEM images were taken at 5kV voltage and 98pA current.

As mentioned earlier, there are three types of structures in the sample – complete hexagonal rings, lines with a gap and junction with spaces. Some examples were randomly selected for checking with SEM from each type of the structure.

For example, in Figure 3.7a, a complete ring can be seen which has around 604nm width and 28 nm arm width. According to the design (Table 3.1), the desired width of the ring and arm are 600nm and 40nm respectively. From the other Figure 3.7b, preferred width of the ring is 800nm where as desired arm width is 40nm. As far as the ring width is concerned, the desired feature size is perfectly achieved in both cases.

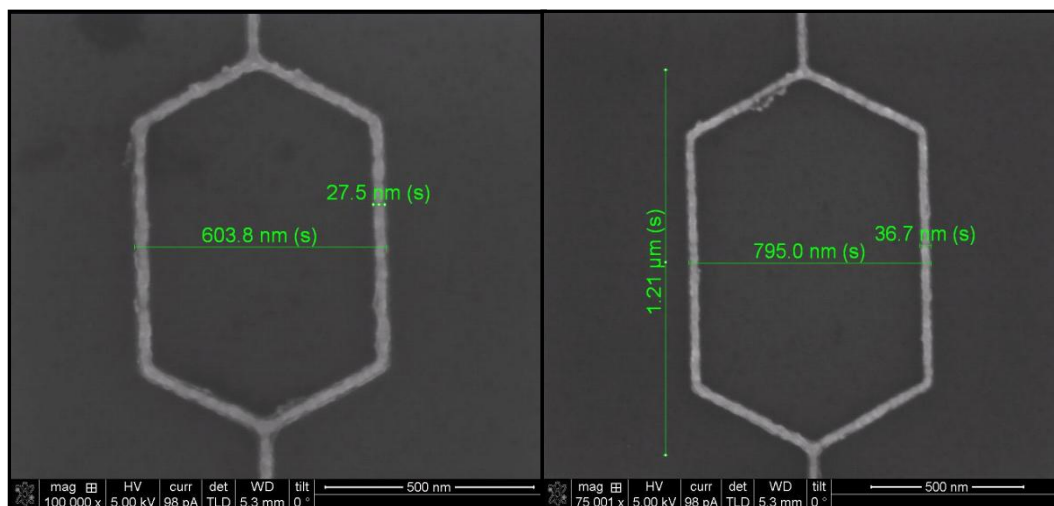


Figure 3.7: SEM image of the Ti/Au Ring a) RingH12, desired design width 600nm and b) RingL12, preferred design width 800nm. Desired arm width is 40nm for both rings.

Then the lines with gaps are shown in Figure 3.8. In both cases the designed arm widths are 40nm and gap sizes are 70nm and 40nm, respectively. It can be said that the results are almost the same in comparison to the desired width.

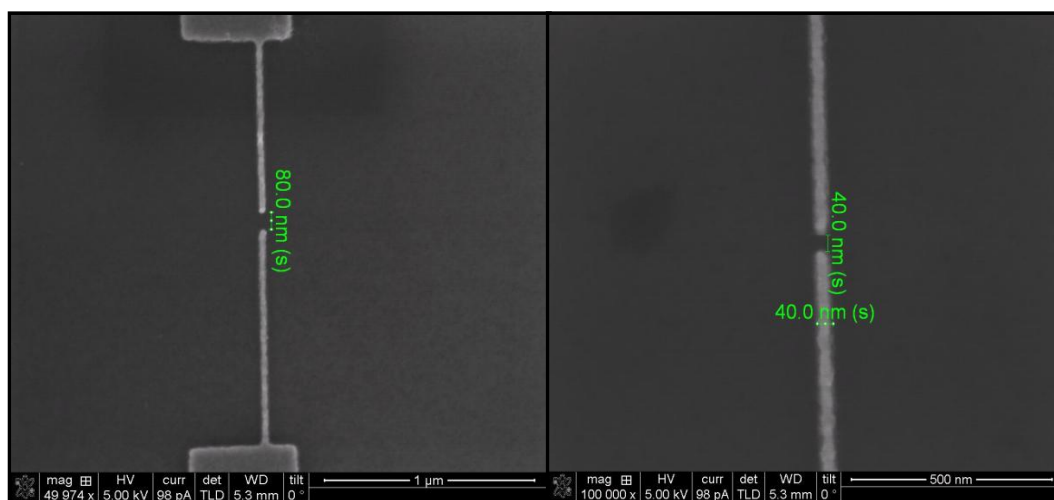


Figure 3.8: SEM images of the Ti/Au lines with gaps a) Line with Gap at K12, desired gap size 70nm and b) line with gap at M12, preferred gap size 40nm. In both cases, 40nm arm widths are desired.

Two examples from junction with space are presented at Figure 3.9. From these two particular SEM images, it is clear that the preferred structure has not achieved (at least for these two cases). As only two images are available, it wouldn't be a wise idea to draw a conclusion about the other junction with space structures.

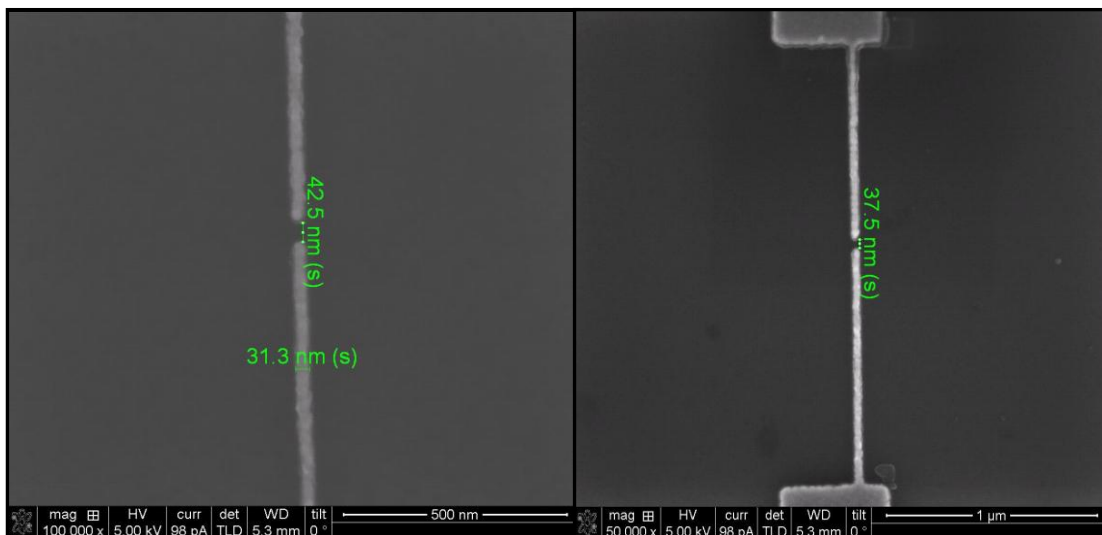


Figure 3.9: SEM image of the Ti/Au Junction with gap structures a) Junction with gap, G12, desired size of the gap is 10nm b) Junction with gap I13, desired gap size 6nm. In both cases, 40nm arm widths are desired.

Overall, desired features except the case of junction with space were achieved during fabrication process. Effectiveness of these features can be verified by different experiments.

## Chapter 4: Measurement Setup

---



It is essential to use a cryogenic setup to observe the Aharonov-Bohm effect. The system consists of some major parts named as – Heliox VL cryostat, Superconducting magnet, measurement electronics and control software. In this chapter, mainly measurement electronics will be discussed.

## 4.1 Heliox VL

Heliox VL is a cryostat made by Oxford Instruments. Using this cryostat, ideally it is possible to go as low as 230 mK [10]. It can hold this temperature for more than 70 hours.

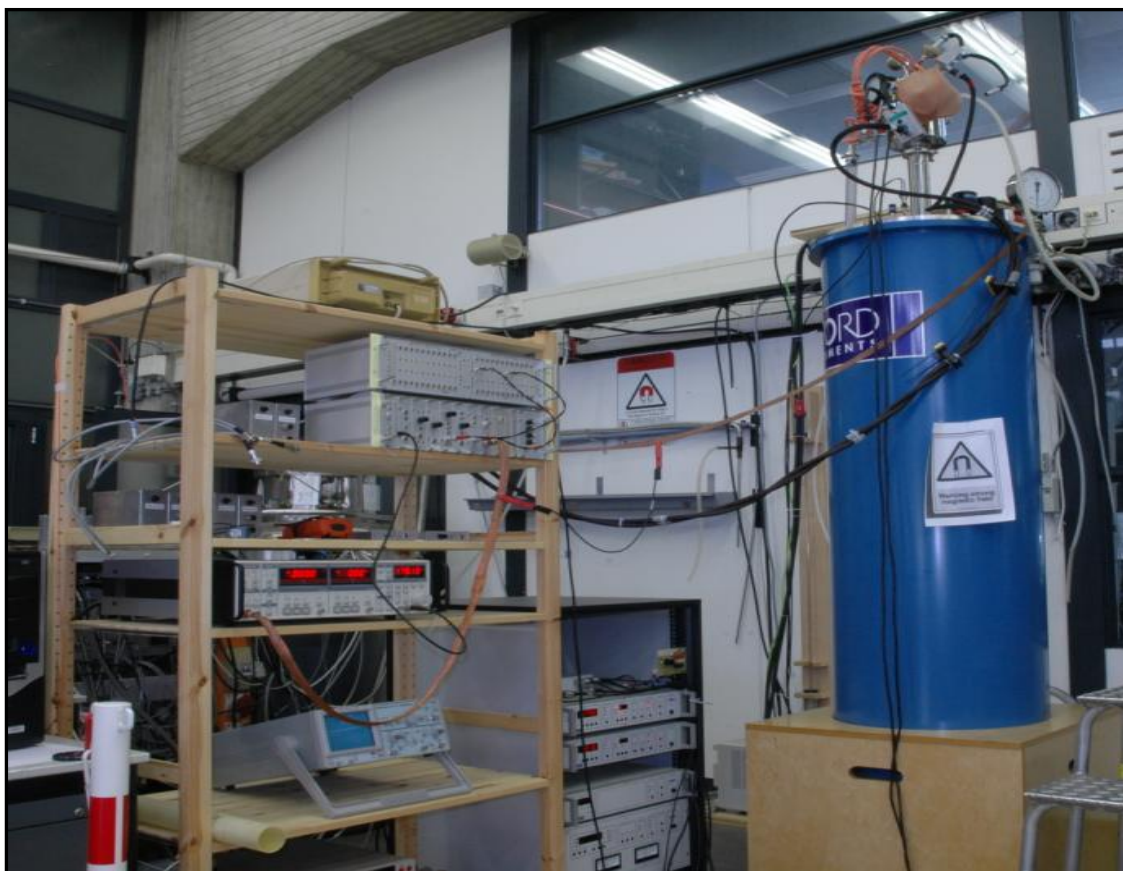


Figure 4.1: The Heliox VL Cryostat from Oxford Instruments with Lock-in SR830 and Delft electronics from TU Delft.

### 4.1.1 Operating Principle of Heliox VL

There are two stages of operation of Heliox VL – condensation and Cooling. In the following Figure 4.2, these two stages are shown[10].

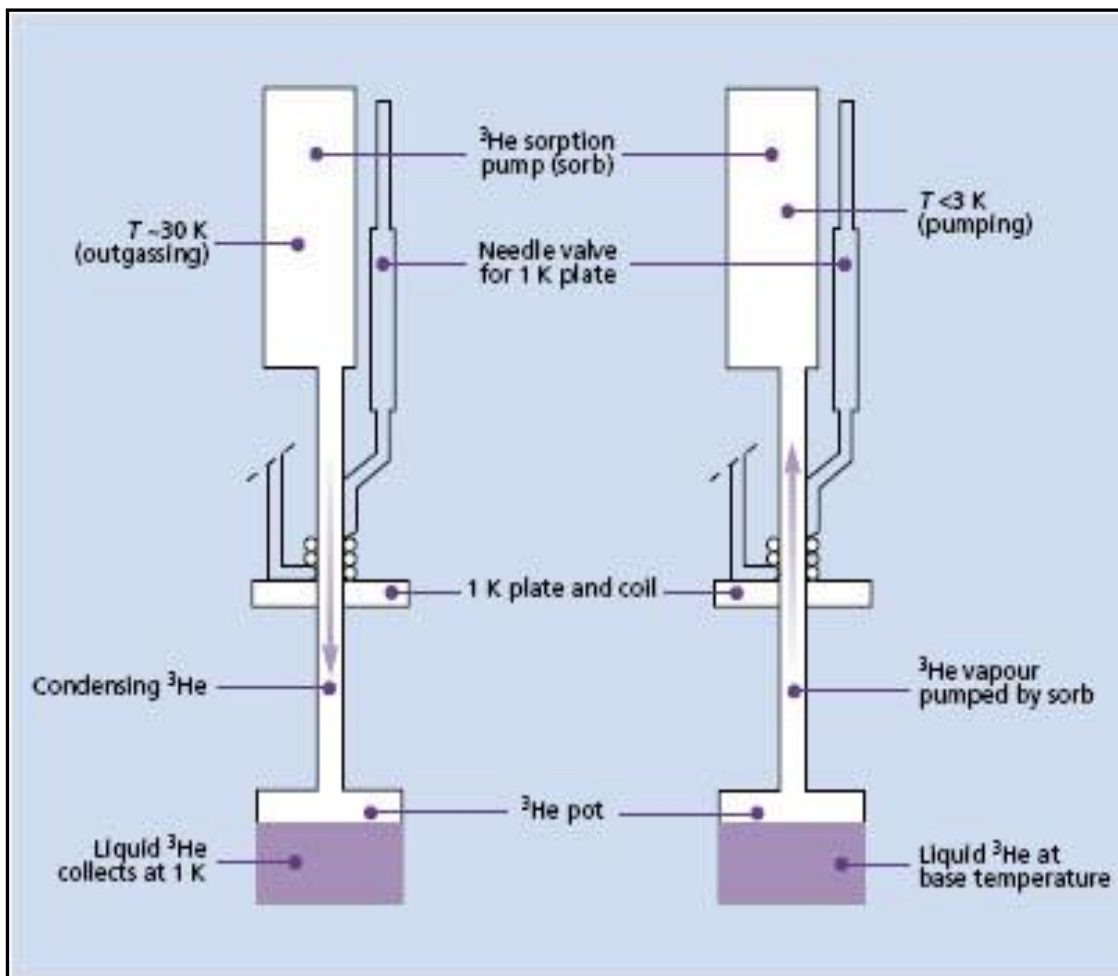


Figure 4.2: Condensation and Cooling of Heliox.

The condensation is done by heating up the sorption pump to about 35 K; at this temperature, it will release all the  $^3\text{He}$  gas adsorbed. This gas is condensed at the 1.5K condenser and collected in the  $^3\text{He}$  pot. In the cooling stage, the sorption pump is cooled; it will start to absorb  $^3\text{He}$  gas and effectively decrease the  $^3\text{He}$  gas pressure above the liquid  $^3\text{He}$ . Due to the evaporation of  $^3\text{He}$  under reduced pressure, the temperature at  $^3\text{He}$  pot is possible to achieve 240 mK. The cold finger is thermally connected with the  $^3\text{He}$  pot. The sample is mounted on the cold finger. As a result, the sample is cooled by exchange heat with the  $^3\text{He}$  pot.

#### 4.1.2 Sample Holder and Wiring

Two custom-made sample holders are made to have magnetic field parallel or perpendicular to the sample. The maximal sample holder size is 11\*11mm. Some capacitors are mounted at the other side of the sample holder. The capacitance is 47nF. So the resistance of the wire about 240 Ohm, a cut of frequency of 14 kHz can be obtained. An image of the holder with bonded wire and cold finger can be found in the following Figure 4.3.

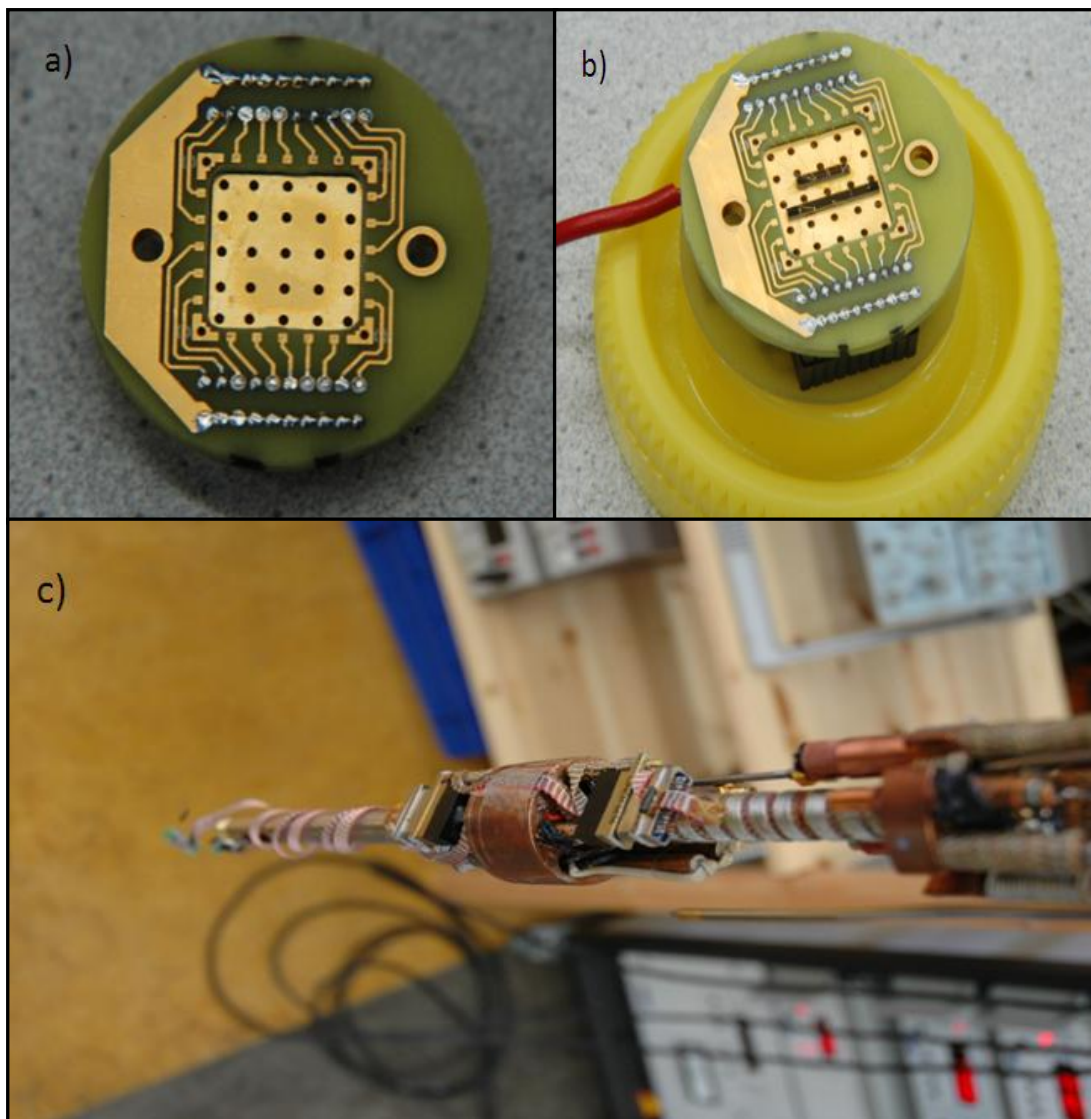


Figure 4.3: Image of a) Sample holder b) Sample holder with bonded wire c) cold finger.

There are 20 bonding pads available for wire bonding (Figure 4.3a). These 20 bonding pads are linked to the connector A at the upper side of the  $^3\text{He}$  pot and the connector B at the lower side of the  $^3\text{He}$  pot. These 20 connections are connected to the Matrix Module, which can be accessed at room temperature. Out of these 20 connections, 14 connections were working properly. So it was possible to bond couple of rings for the measurement. There might be some problem with the other connections such as broken connection wire or inappropriate soldering etc.

In the previous study [3], a sample holder was used which had 2 cm of single wires. Under the presence of the magnetic field, the movement of the single wires from the vibration caused random current noise. It was hard to distinguish AB oscillations out of this noise. So to improve this situation and to avoid the noise, this new sample holder was designed where the voltage probe and current supply are in the same twisted pair. The sample holder is also mounted at the cold finger. All the wiring of the new sample holder was completed successfully.

## 4.2 Measurement Electronics

The measurement electronics consists of isolation amplifiers, current source and voltage amplifier. LabView-based software was used to control the measurements. These Delft made electronics are shown in Figure 4.4.

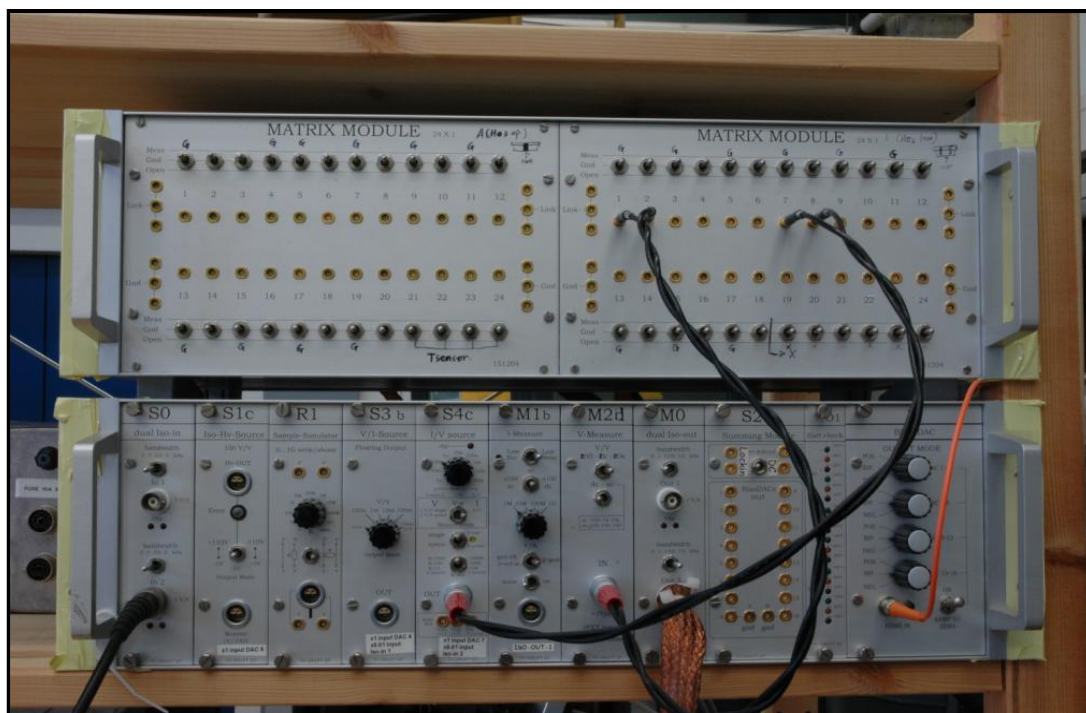


Figure 4.4: Delft-made electronics. Matrix Module, Isolation amplifier, Voltage amplifier (M2d) and current source S4c.

Isolation amplifiers are used to isolate external sources like lock-in amplifiers. It can also separate the external measurement units (such as digital multimeters) from the battery driven measurement electronics.

The name of the current source is S4C. It is possible to drive it via a DAC or the output of a lock-in amplifier. Its current ranges from 10 nA/V to 20mA/V. During the measurement, current mode has used with  $R_{out}$  switch set at 1000 times of  $R$  which corresponds to 1000times amplification. This condition gives the highest accuracy.

Two different voltage measure modules were used as voltage amplifier –M2b and M2d. M2b has a low  $1/f$  noise, but M2d has even lower  $1/f$  noise. However, M2d have no DC stability. That is why M2b has used during the DC resistance measurement at room temperature. The M2d voltage amplifier was used during magnetoresistance measurement since extremely low  $1/f$  noise is essential to observe AB oscillations.

Noise specifications of the voltage amplifiers are shown in Table 2.1.

Table 4.1: Voltage Amplifiers specifications.

	<b>M2d</b>	<b>M2b</b>
<b>Input Noise Voltage</b>	0.8nV/Sqrt Hz>10Hz	2nV/sqrt Hz>10Hz
<b>Input Noise Current</b>	50fA/sqrtHz	50fA/sqrtHz
<b>Input Bias Current</b>	<50pA	<5pA
<b>Temp Drift</b>	<5uV/C	<2uV/C
<b>Bandwidth</b>	200kHz..10kHz (gain=100...100K)	200kHz..10kHz (gain=100..10K)

Calculated voltage noise is equal or lower than 10 nV. During measurement, voltage noise was also calculated. It was found that for the RingH12, the noise was 0.5nV where as for RingD12, the noise was 0.9nV. So signal to noise ratio is low enough for a good measurement.

### 4.2.1 Lock-in SR830

It is known from the Fourier theorem that it is possible to present any input signal as the addition of numerous sine waves of different amplitudes, frequencies and phases. A SR830 amplifier uses a pure sine wave to multiply the signals at the reference frequency. This reference frequency multiplies all the components of the input signals. The product of this multiplication Yields a DC output signal proportional to the component of the signal whose frequency is exactly locked to the reference frequency. The low pass filter (which follows the multiplier) shows the averaging which removes the products of the reference with components at all other frequencies.

Some features of SR830 Lock-in amplifier were used during measurement like Time Constant, Sensitivity, line and 2\* line filtering etc. Some of the important parameters are also described. During different measurements, these parameters were changed or varied to achieve the optimal condition. All these measurement parameters values for different measurement can be found in the Appendix 4.

#### Sensitivity

The sensitivity depends on the voltage output from the voltage amplifier M2d. It was either 200mV or 500mV during the different measurement.

#### **R**

This is the actual voltage calculated based on the phase ( $\theta$ ) and output from channel X and Y.

#### X and Y Noise

Before measurement started, the noise was checked in channel X and Y. The unit of noise was in mV. Just after changing the certain parameters (such as

sensitivity or R) for different experiments, X and Y noise became instable. It took couple of minutes to stable the value of both noises. Generally it stabled between 0.00mV to 0.03mV during different measurements.

### **Phase ( $\theta$ )**

This adjusts the reference phase shift. It was zero during all measurements.

### **Amplitude**

This button represents the sine amplitude of the output signal from the lock-in amplifier.

## **4.3 Effective Electron Temperature**

In the cryogenic measurements, the electrons experience noise. As a result, the effective electron temperature can be higher than the bath temperature. This could create a problem for observing AB oscillations, due to decreased coherence length.

To determine the actual electron temperature, one experiment with Kondo sample was performed. The resistance vs.  $\log T$  was plotted in Figure 4.7. Theory suggests resistance vs.  $\log T$  is linear. However, in Figure 4.7, a bending behavior near base temperature was observed.

Temperature sensor showed 260mK. On the other hand the measured resistance at 260mK corresponds to 360mK according to the liner fitting on the data. So during measurement, the minimal effective electron temperature is around 360mK. Inserting heavy RC filtering at low temperature (with a cut off frequency anything less than 500Hz) could lower the effective electron temperature further.

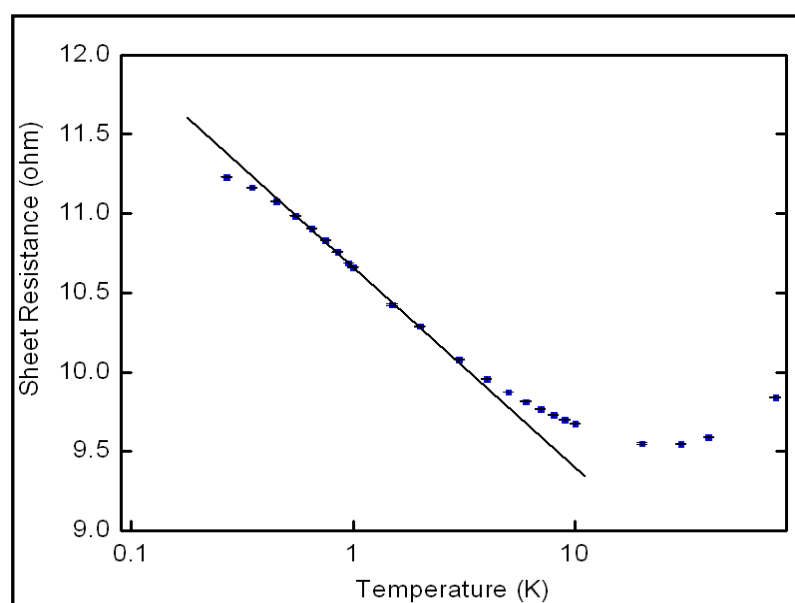


Figure -4.7: Temperature vs. Resistance of a Kondo Sample.

## 4.4 Measurement Diagram

A block diagram for all the measurement is represented in the Figure 2.8.

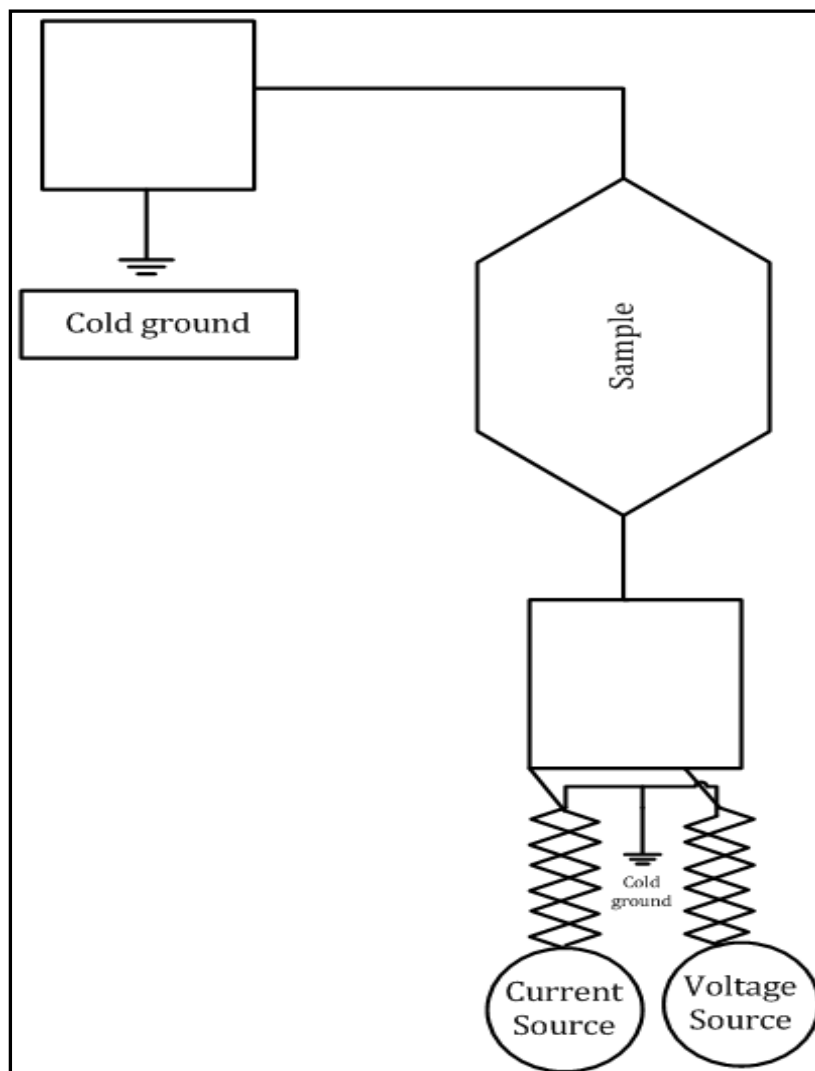
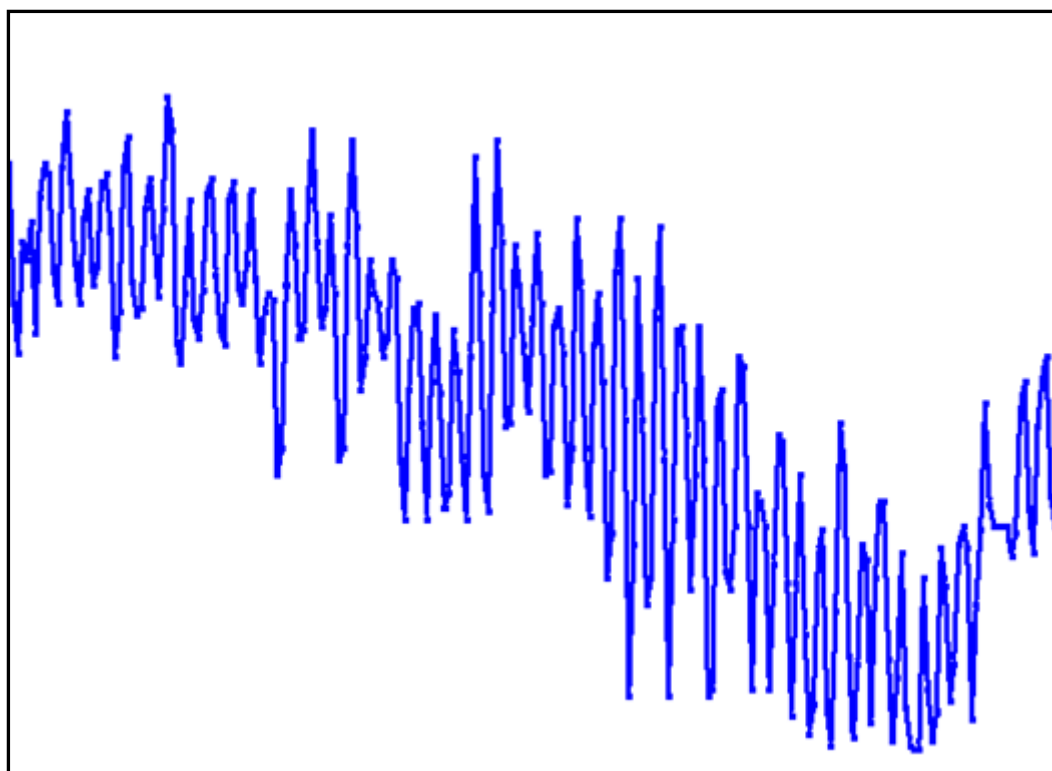


Figure 4.8: Block diagram for the two point measurement.

There are two twisted pairs to access a terminal of each ring. In this way, the random current noise due to the vibrating wire in magnetic field can be cancelled out. One twisted pair is for current supply and the other twisted pair is for voltage probing. One wire in the twisted pair is connected to a terminal of the ring whereas the other wire is attached to the cold ground in order to avoid thermal voltages between ground levels. The other terminal of the ring is also attached to the cold ground. This connection diagram provides the necessary configuration for the two-point measurement.

## Chapter 5: Results and Discussion

---



In low temperature measurements, the thermal energy plays an important role. The value of the electron energy should be lower than thermal energy. ( $k_B T = \text{Boltzman constant} \times \text{Temperature} = 1.3806503 \times 10^{-23} \text{m}^2 \text{kg s}^{-2} \text{K}^{-1} \times 250 \text{mK} = 21.75 \mu\text{eV}$ ) This rule was used to determine the maximum excitation current for the measurements. For example, if the sample has a resistance of 500ohm, maximum excitation current at 250mK would be around 43.5nA (Considering  $I \times R \leq 21.75 \mu\text{eV}$ ).

Three rings from row D(400nm) and one ring from row H(600nm) were chosen for wire bonding. First these rings were bonded with Al wire. To verify a proper connection to the sample, the resistance of the sample was measured at room temperature. After cooling down, the magnetoresistance of the sample was measured in a field regime between -7T and +7T. After this full range measurement, several small regimes were chosen where the AB oscillations were most appealing. A few measurements were taken in these regimes at various temperature and excitation current to investigate the temperature and excitation current dependence of the AB oscillations.

Then sample was taken out from the Heliox. It was diced into several small pieces (10\*1mm) for the NP insertion. Rotation speed of the saw was 2500k rpm, feed speed was 5mm/s. Afterwards couple of rings from Row D and H were bonded using gold wire and some measurements were repeated. Detail bonding map can be found in Appendix 2.

The data analysis started by plotting resistance vs. magnetic field. A polynomial fit with the order of 9 was applied to the data. Afterwards, polynomial fitting was subtracted from the original data. In case any oscillation was observed, a fast Fourier transfer (FFT) will be performed on the resulting data to extract the periodicity of the oscillation. All the data presented in this chapter were processed using this procedure.

The expected value of the AB oscillation period and the aspect ratio of the rings are listed in Table 5.1. The detailed calculation procedure can be found in Appendix 3.

Table 5.1: Aspect Ratio and theoretical AB oscillation period of the rings.

Ring	Width of the Ring (nm)	Aspect Ratio	Theoretical Period (mT)
B	300	1.75	37.0
D	400	2.38	20.7
F	500	3.00	13.0
H	600	3.63	9.2
J	700	4.25	6.5
L	800	4.88	5.0
N	900	5.50	4.0
P	1000	6.13	3.0
R	1000	6.13	3.0

## 5.1 Resistance Measurements

After loading the sample, the resistance of the rings was measured to check the connections. The resistance was measured both at room temperature and base temperature (260 mK). Two rings out of four showed reasonable resistances as listed in Table 5.2. A temperature goes down, resistance decreased due to the scattering effects. The resistance decreased as temperature goes down. This behavior is expected as at low temperature, generally resistance decreases due to the electron's scattering effect. The rest of the rings were open, which may due to the structural defects.

Table 5.2: Resistance of the rings at room temperature and base temperature. Standard error is shown inside the bracket.

Ring	Resistance (ohm) at room temperature with standard error	Resistance (ohm) at 260mK with standard error
Ring D12	725.66 (0.0715)	515.29 (0.0452)
Ring H12	453.60 (0.1207)	306.75 (0.0528)

## 5.2 AB Oscillations

First measurements were taken on ring H12. The magnetic field was swept from -5T to 5T with a step size of 2mT; the excitation current was 30 nA and temperature was 262mK. Some good oscillation region was checked. The detail parameters of all the experiments can be found in Appendix 4. The magnetoresistance of ring H12 before and after subtracting the polynomial fit in the field regime -4.2T to -2.7T is plotted in Figure 5.1 and Figure 5.2, respectively.

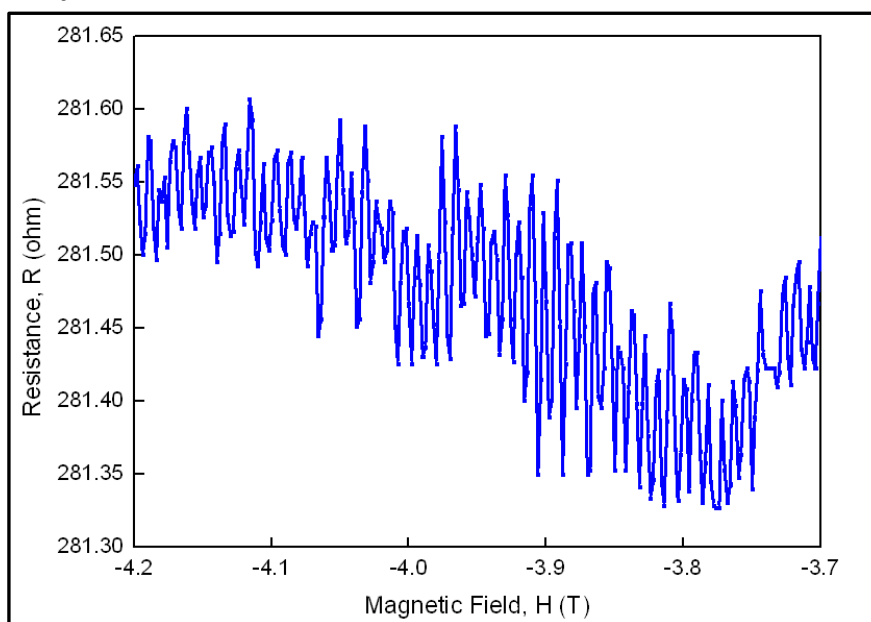


Figure 5.1: Magnetoresistance of ring H12 before subtracting the polynomial fit in the field regime -4.2T to -3.7T with a step size of 2mT. The excitation current is 30nA and temperature is 262mK.

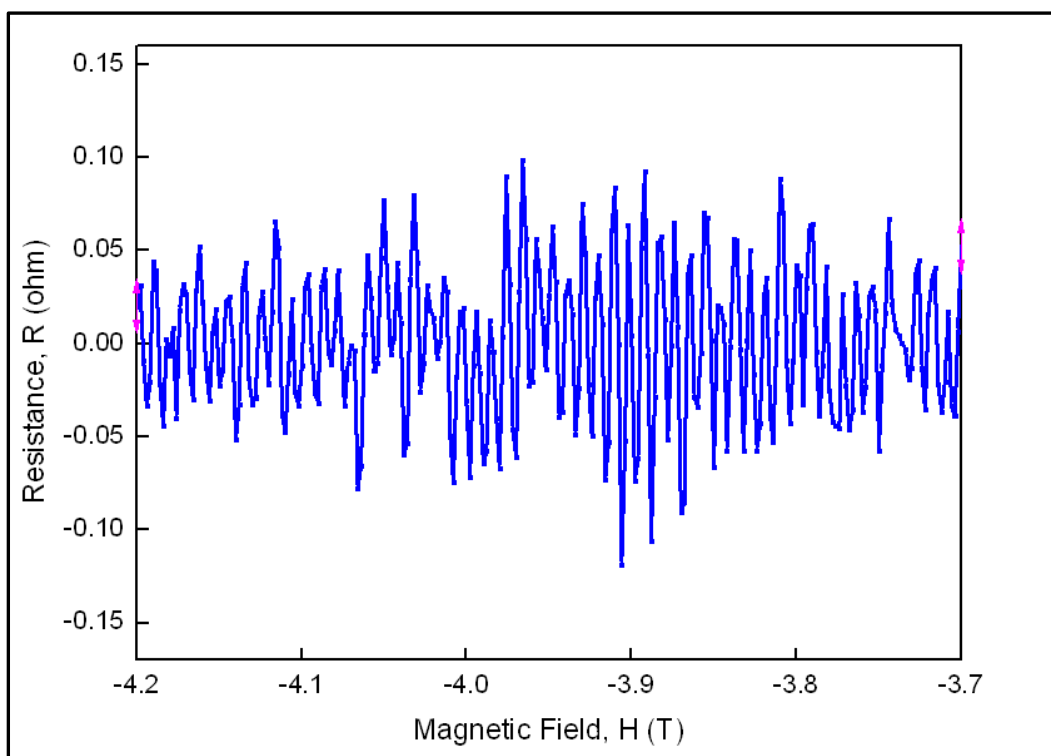


Figure 5.2: Magnetoresistance of ring H12 after subtracting the polynomial fit in the field regime -4.2T to -3.7T with a step size of 2mT. The excitation current is 30nA and temperature is 262mK.

Clear AB oscillation has been observed in Figure 5.1 and 5.2. Then the FFT has been performed on the data in Figure 5.2 and plotted in the Figure 5.3.

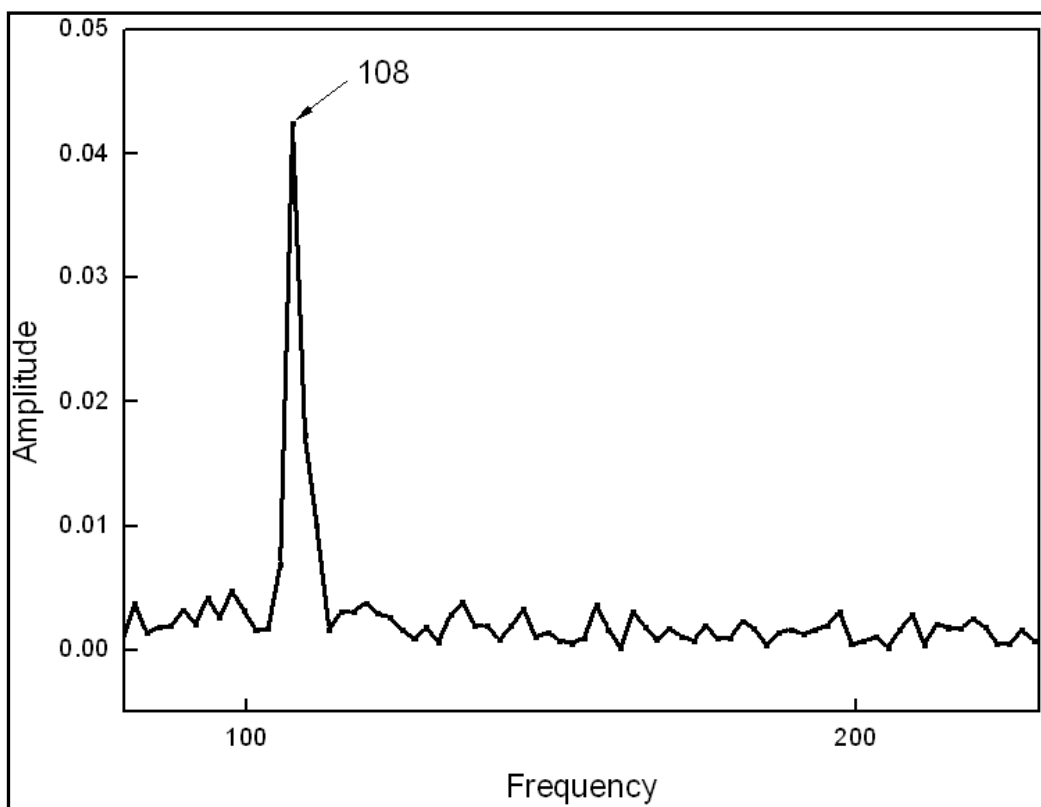


Figure 5.3: FFT of the data presented at Figure 5.2. Peak position is 108.

A clear peak at position 108 was found. It corresponds to an oscillation period of 9.3mT (calculated by  $1/108$ ) which is very close to the theoretical calculation (9.2 mT). This period is reproducible across different magnetic field intervals.

For example, magnetoresistance of this ring after background subtraction in the field regime -1.7T to -1.2T (smoothed for 5 points) is plotted in Figure 5.4a; corresponding FFT is plotted in Figure 5.4b. The observed AB period is 9.3 mT. AB oscillations become more evident than that of the previous one. Peak position and AB period is unchanged.

During this measurement, only  $h/e$  peak was observed. This is due to the resolution of the measurement was not high enough to observe any  $h/2e$  peak.

Based on further analysis, the oscillation is most appealing in the regime from -1.7T to -1.2T. This regime was chosen for a couple of other experiments (for example: temperature and excitation dependence) for this particular ring.

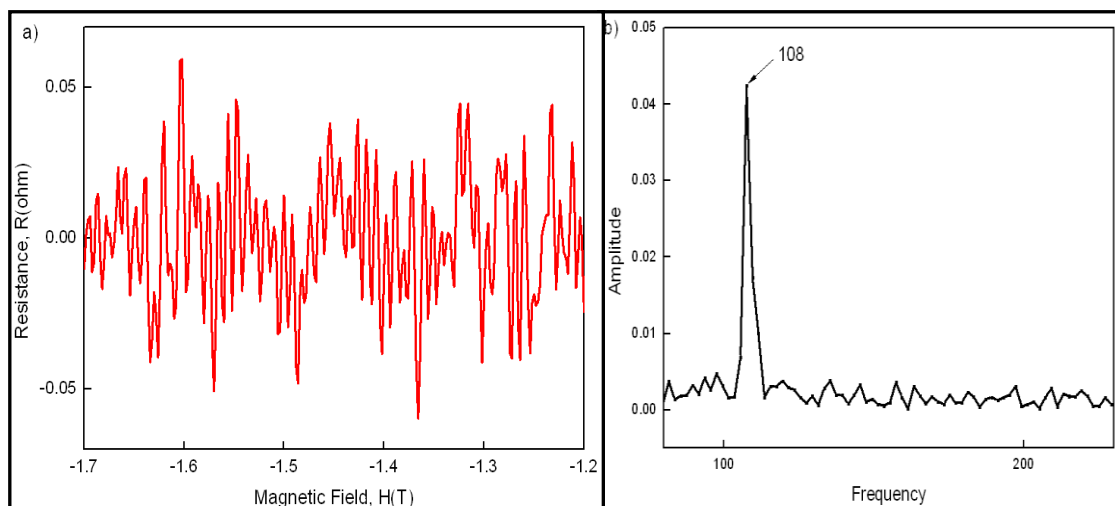


Figure 5.4: a) Magnetoresistance of ring H12 after subtracting the polynomial fit in the field regime -1.7T to -1.2T with a step size of 2mT (smoothed for 5 points). The excitation current is 30nA and temperature is 262mK. b) FFT of the data presented in Figure 5.4a. Peak position is at 108.

Later,  $h/2e$  peak was observed for a smaller step size (0.4mT); corresponding FFT is presented at Figure 5.5.

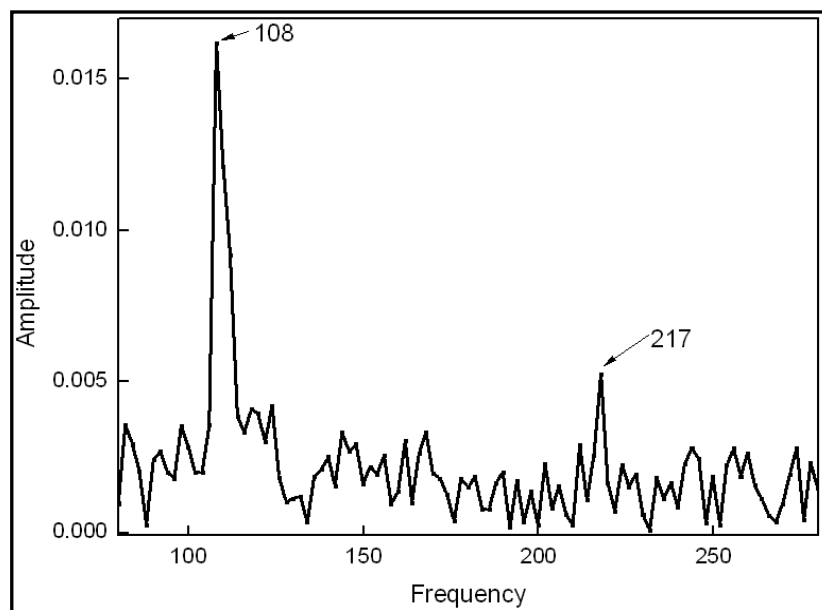


Figure 5.5: FFT Results of the magnetoresistance of ring H12 in the field regime -1.7T to -1.2T with a step size of 0.4mT. The excitation current is 30nA and temperature is 261mK.

It was also possible to observe the AB oscillation for a different ring (D12, 400nm width). At the beginning a full range measurement was taken by sweeping the magnetic field from -7T to 7T and 7T to -7T with a step size of 1mT at base temperature ( $\sim 262\text{mK}$ ); the excitation current was 30nA. After analyzing the data, most appealing oscillation regime was found between 5T to 5.5T. Magnetoresistance of ring D12 after subtracting the polynomial fit in the field regime 5.5T to 5T with a step size of 1mT (smoothed for 5points) is plotted in Figure 5.6.

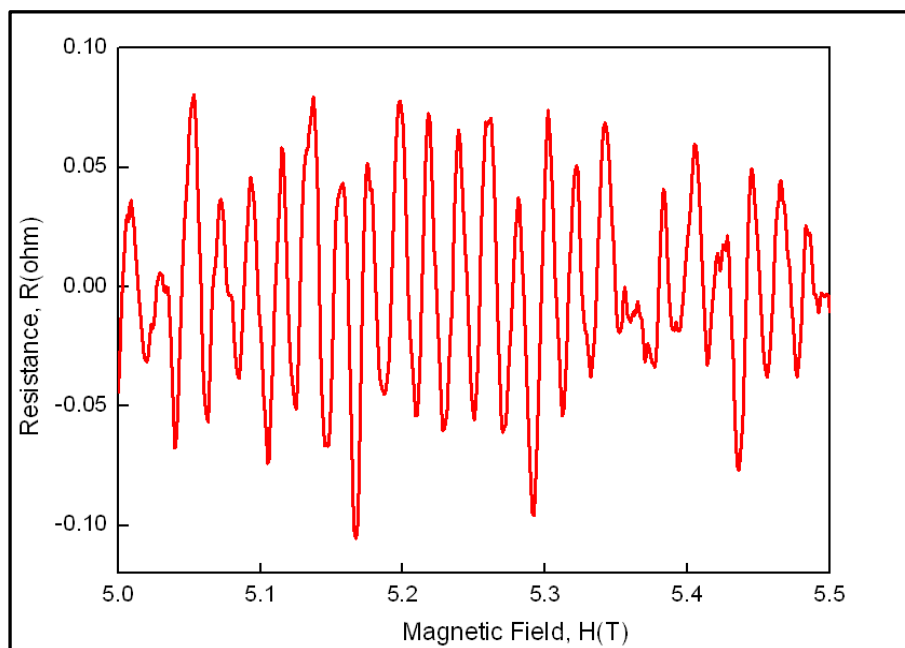


Figure 5.6: Magnetoresistance of ring D12 after subtracting the polynomial fit in the field regime 5T to 5.5T with a step size of 1mT (smoothed for 5points). The excitation current is 30nA and temperature is 262mK.

The periodical oscillation of the magnetoresistance is clearly observed from the Figure 5.6. This magnetic field regime was chosen for a couple of other experiments (such as temperature and excitation dependence) for this particular ring.

To extract the period, a FFT was performed on data in Figure 5.6 and plotted in Figure 5.7. A clear peak was found at the position of 47.9, which corresponding to  $h/e$  oscillations with a period of 20.8mT. This value is in agreement with the theoretical value (20.7 mT) showed earlier in this chapter. The AB period of this ring is also reproducible across different ranges.

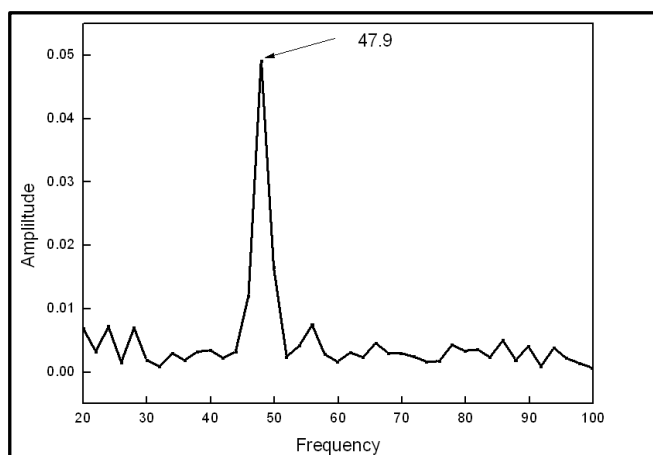


Figure 5.7: FFT of the data presented in Figure 5.6. Peak position is at 47.9

The AB oscillations should be coincided in the same magnetic field regime regardless the sweeping direction of the magnetic field. To verify this issue, a measurement was taken in a small range (200 mT) of magnetic field to check whether the oscillations coincide with each other. Magnetic field was swept at both directions (5.5T to 5.3T and 5.3T to 5.5T) with a step size of 1mT. The excitation current was 30 nA and temperature was 261mK. Corresponding results are plotted in Figure 5.8.

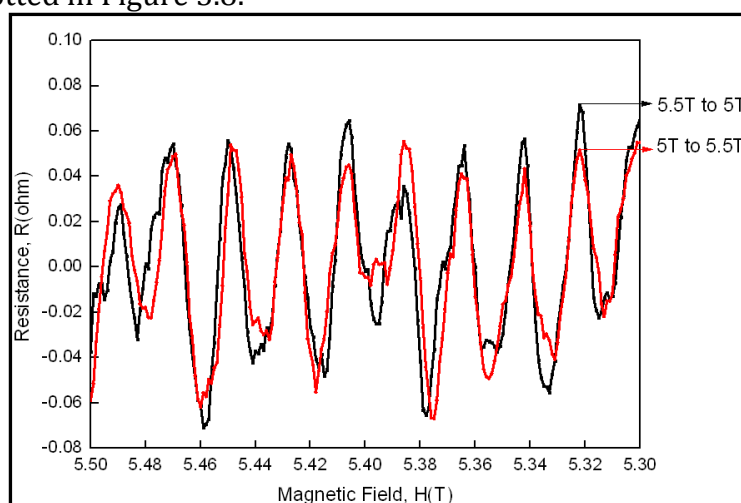


Figure 5.8: Magnetoresistance of ring D12 after subtracting the polynomial fit in the field regime 5.5T to 5T (black) and 5T to 5.5T (red) with a step size of 1mT (smoothed for 5points). The excitation current is 30nA and temperature is 261mK.

### 5.3 Temperature dependence of AB oscillations

At first, temperature dependence of AB oscillations for ring H12 was checked. Measurements were taken at the magnetic field regimes chosen earlier (-1.7T to -1.2T and -1.2T to -1.7T) with a step size of 0.4 mT at different temperature with 30nA excitation current. Magnetic field was swept in both directions. The magnetoresistance of ring H12 at different temperatures in the field regime -1.6T to -1.2T is plotted in Figure 5.9.

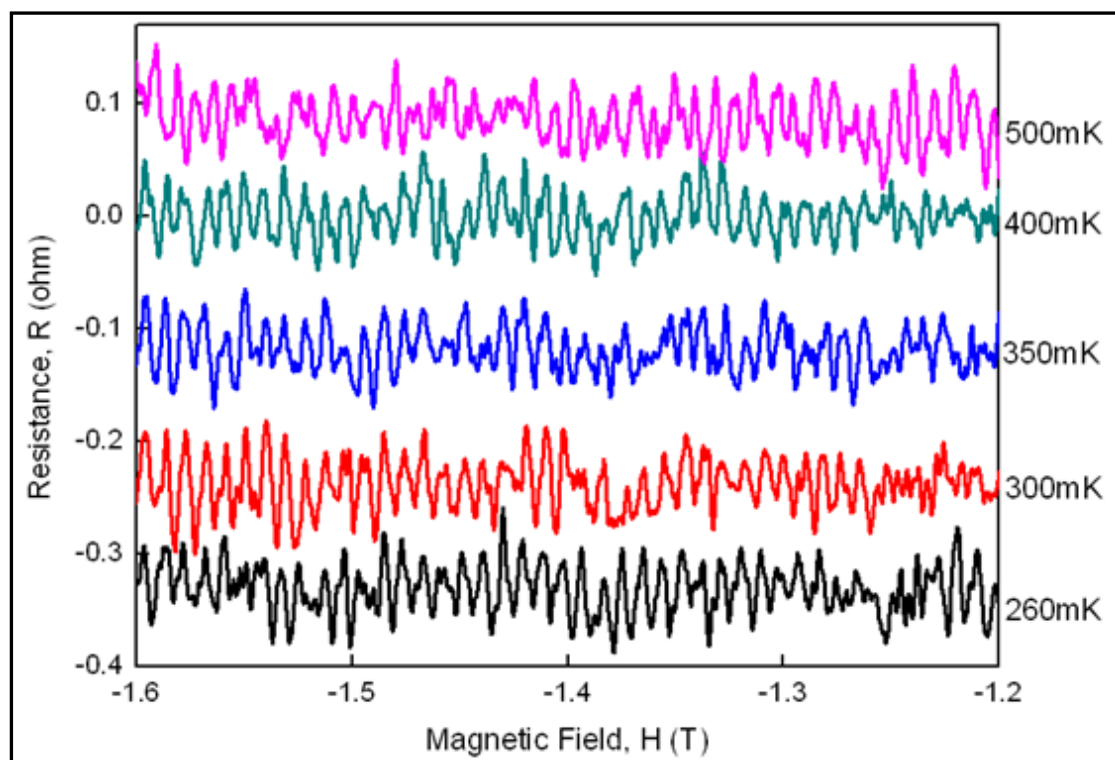


Figure 5.9: Temperature dependence magnetoresistance of ring H12 after subtracting the polynomial fit in the field regime -1.6T to -1.2T with a step size of 0.4mT (smoothed for 5points). The excitation current is 30nA.

Periodical oscillations are clearly observed at base temperature (260mK). It can be seen that the oscillation is significant till 350mK. Further increasing the temperature, oscillation quality became less significant. The period obtained ( $\sim 9.3$ mT) from all these measurements are consistent. It can be said that AB oscillations are not completely temperature dependent for this particular ring.

Next, temperature dependence of AB oscillations for ring D12 was checked. To do this, resistance measured at different temperature starting from 260mK to 400mK by sweeping the magnetic field from 5.5T to 5T with a step size of 1mT. Excitation current was. Magnetoresistance of ring D12 at different temperatures are plotted in Figure 5.10.

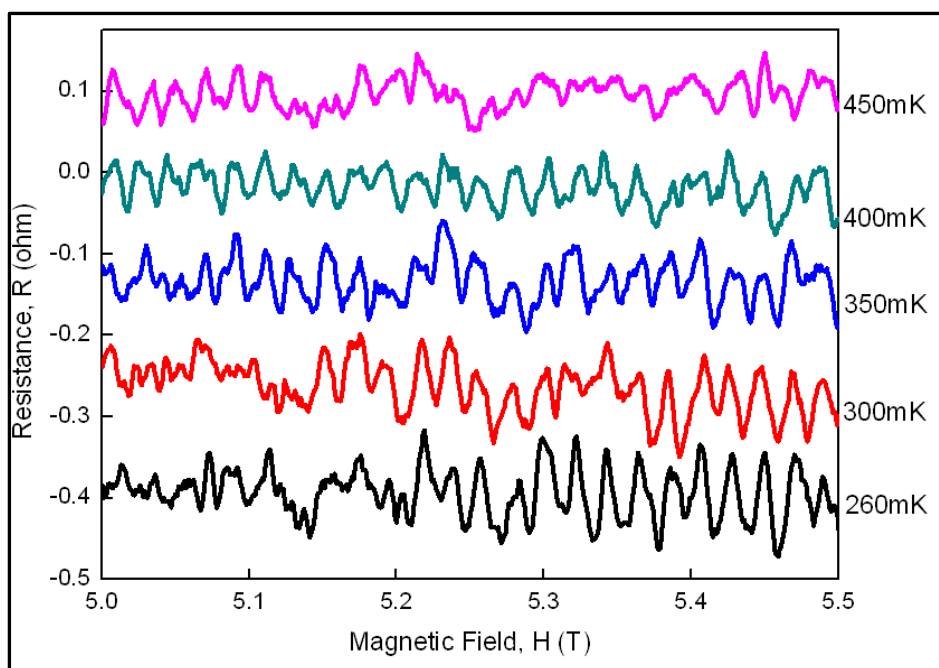


Figure 5.10: Temperature dependence magnetoresistance of ring D12 after subtracting the polynomial fit in the field regime 5.5T to 5T with a step size of 1mT (smoothed for 5points) at different temperature. The excitation current is 30nA.

From Figure 5.10, periodic AB oscillations are observed from base temperature till 450mK. At different temperature the AB period 20.8mT was reproducible. At 300mK, clear  $h/e$  and  $h/2e$  peaks are observed in the FFT (Figure 5.11).

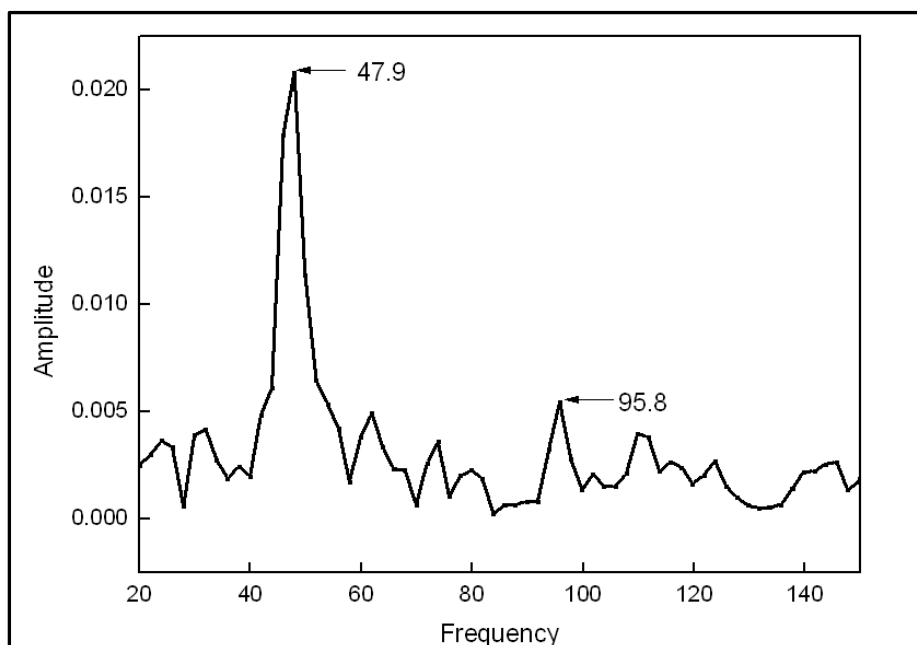


Figure 5.11: FFT Results of the magnetoresistance of ring D12 in the field regime 5.5T to 5 T with a step size of 1mT. The excitation current is 30nA and temperature is 300mK.

Amplitude maximum and amplitude average are defined as the maximum amplitude and average amplitude of AB oscillations for a particular temperature. These two values as a function of different temperatures for the above measured field are plotted in the Figure 5.12. These values are determined manually from the magnetoresistance plot of different temperatures for a particular field regime.

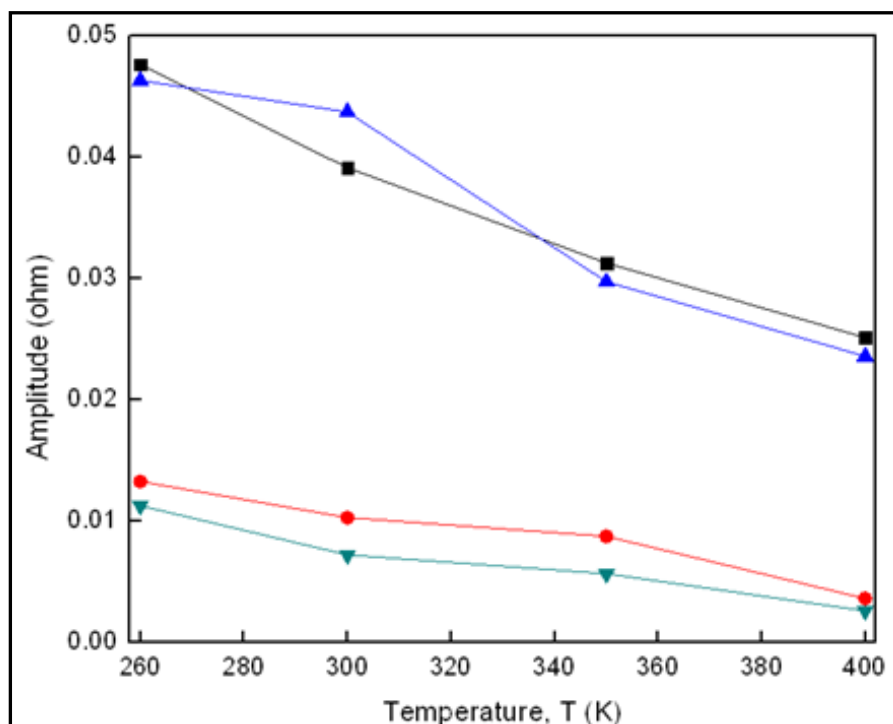


Figure 5.12: Comparison of amplitude maximum and amplitude average at different temperature for ring D12. Black and blue plots correspond to the amplitude maximum for the field sweep from 5.5T to 5T and from 5T to 5.5T respectively. Red and green plots correspond to the amplitude average for the field sweep from 5.5T to 5T and from 5T to 5.5T.

The trend is that the AB oscillation amplitude decreases by increasing temperature. This behavior can be related with the coherence length. Generally the coherence length increases if temperature decreases, as a result the amplitude of AB oscillation increase. This is due to the fact that scattering events are present. Overall temperature has insignificant effect on amplitude of AB oscillations.

#### 5.4 Excitation Current Dependence of AB oscillations

First, the excitation current dependence of the AB oscillations was checked for ring H12. To investigate this, excitation current was varied from 10nA till 35nA in the field regime -1.7T to -1.2T with a step size of 0.4mT. The temperature was  $\sim 260$ mK. The magnetoresistance at different excitation current in the field regime -1.7T to -1.3T is plotted in Figure 5.13.

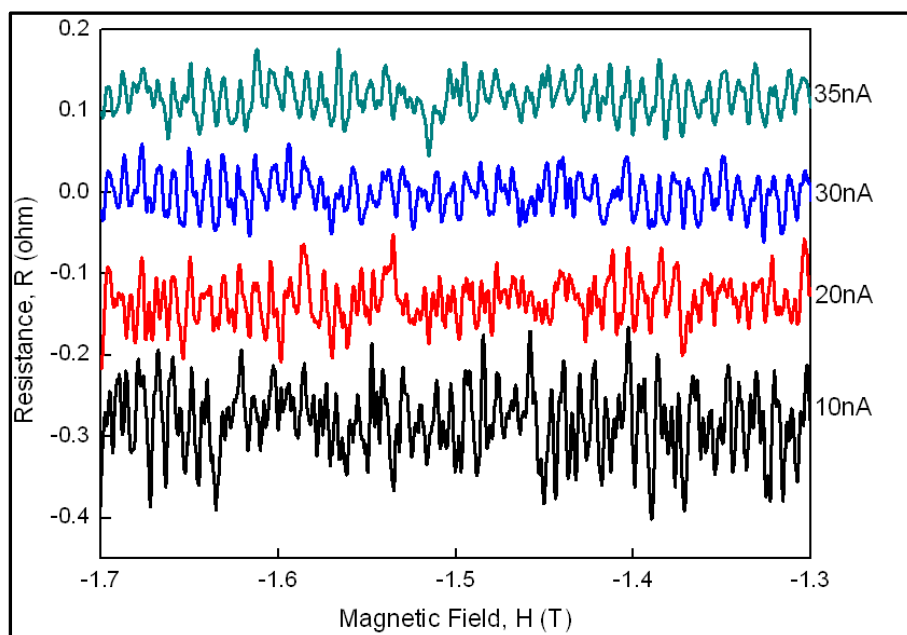


Figure 5.13: Excitation current dependence of magnetoresistance from ring H12 after subtracting the polynomial fit in the field regime -1.7T to -1.3T with a step size of 0.4mT (smoothed for 5points). Temperature is  $\sim 260$ mK.

Oscillations are clearly observed at different excitation currents. It can be seen that the oscillation become more evident when the excitation current increases. The AB amplitude is larger for lower excitation currents. Also the period obtained ( $\sim 9.3$ mT) from all these measurements are very close to the theoretical calculation.

Amplitude maximum and amplitude average vs. different excitation currents have plotted in Figure 5.14. Both amplitudes decrease with increasing excitation current.

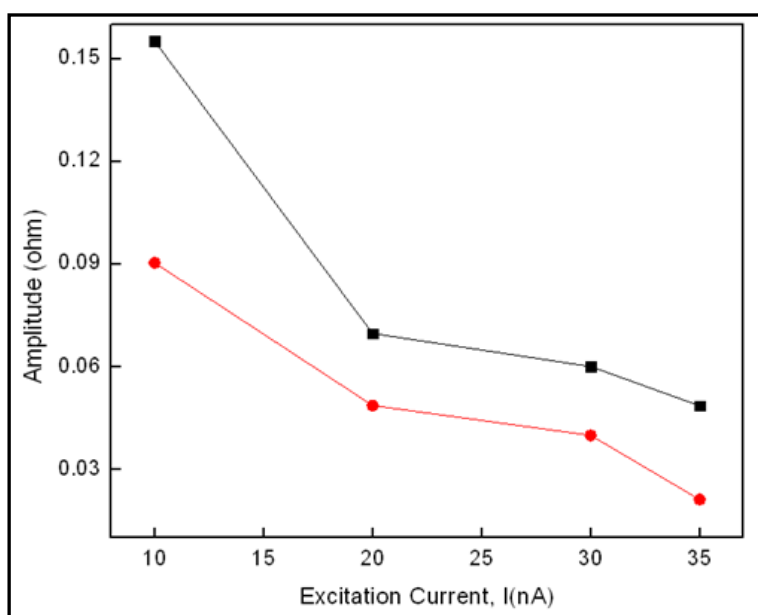


Figure 5.14: Comparison of Amplitude Maximum (black) and Amplitude Average (red) at different excitation current for ring H12. The temperature is  $\sim 260$ mK.

Excitation current is also related with the effective electron temperature or energy of the electron at that particular current. So energy corresponding to the different excitation currents is calculated in Table 5.3. At 260 mK, the thermal energy  $k_B T$  is 22.4  $\mu\text{eV}$ .

Table 5.3: Energy corresponds to the different excitation current.

Excitation Current (nA)	Energy ( $\mu\text{eV}$ )
10	5.15
20	10.32
30	15.54
35	18.03

From the Table 5.3, it can be said that if excitation current increases, energy also increases. So amplitude increases with the decreasing energy. For all excitation current, electron energy is lower than  $k_B T$ . That is why it was possible to get AB oscillations for all these ranges of excitation currents.

Excitation current dependence was also checked for the ringD12. In this experiment, excitation current varied from 10nA till 40nA in the field regime 5.5T to 5T with a step size of 1mT. The temperature was  $\sim 260\text{mK}$ . Corresponding results are plotted in the Figure 5.15.

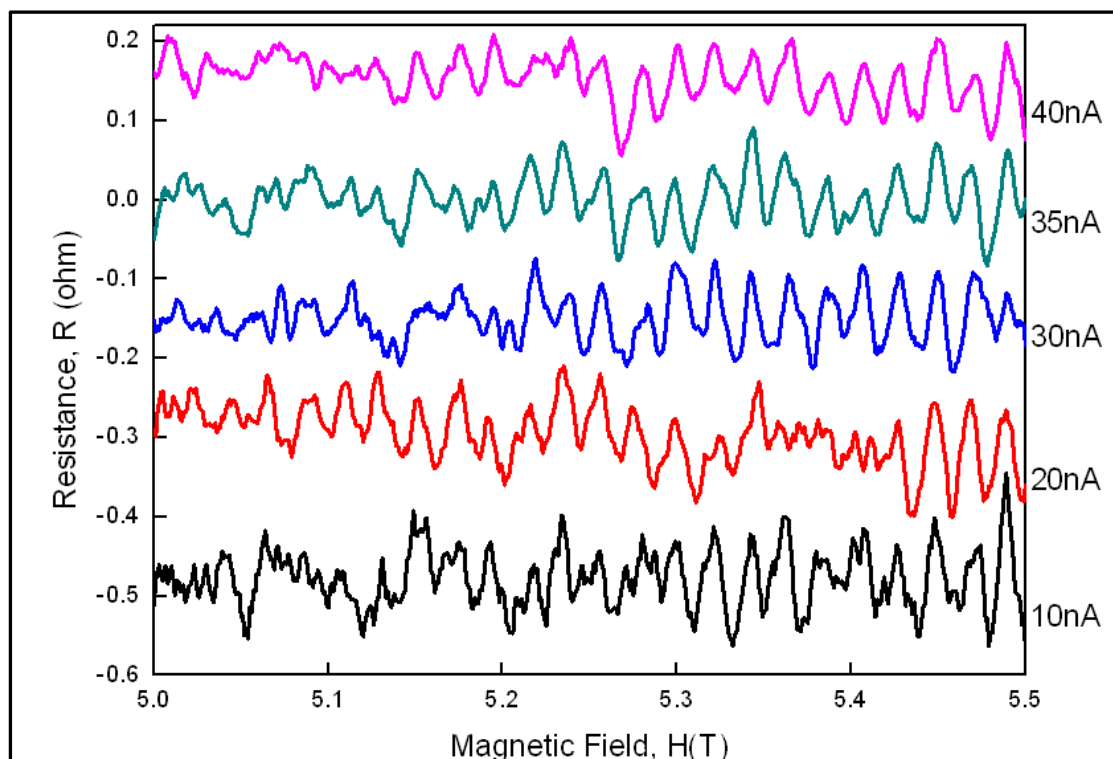


Figure 5.15: Excitation Current dependence of magnetoresistance from ring D12 after subtracting the polynomial fit in the field regime 5T to 5.5T with a step size of 1mT (smoothed for 5points). Temperature is  $\sim 260\text{mK}$ .

Clear periodic AB oscillations can be seen from the Figure 5.15. The amplitude becomes less for higher currents. Observed AB period 20.8 mT was reproducible at different excitation current.

Amplitude max and Amplitude Avg. as a function of different excitation currents for the above mentioned field are plotted in the Figure 5.16. The trend is the amplitude decreases by increasing excitation current. This is due to the increasing electron energy which is in agreement with the theory and in agreement with the previous measurement on the other ring H12 (Figure 5.14).

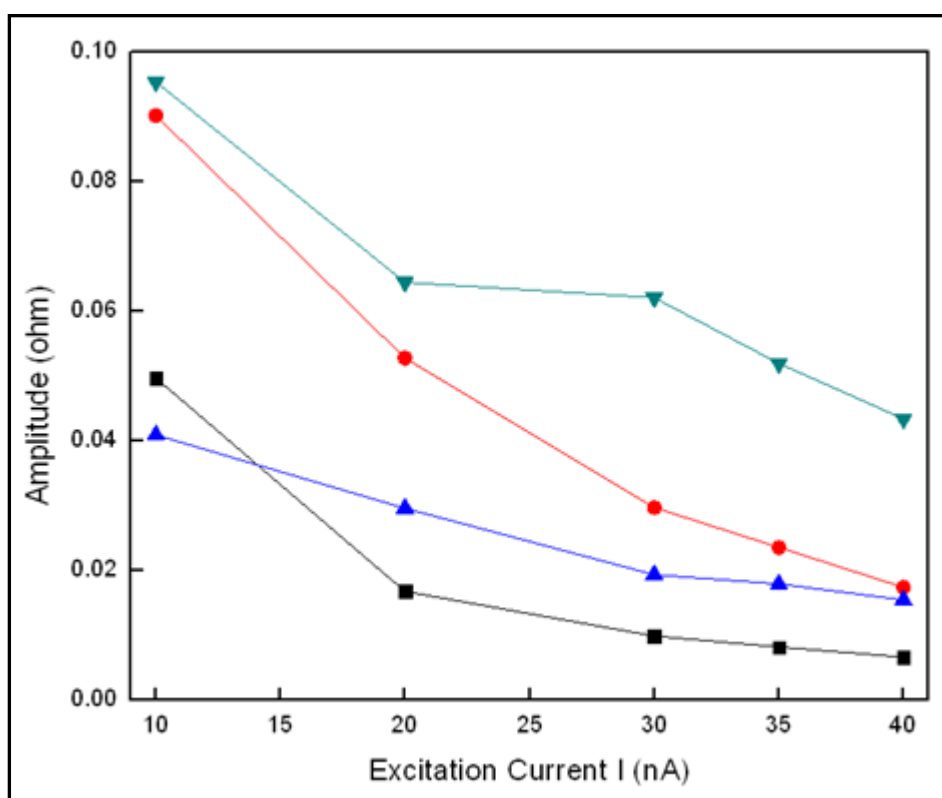


Figure 5.16: Comparison of amplitude maximum and amplitude average at different excitation current for ring D12. Green and red plots correspond to the amplitude maximum for the field sweep from 5.5T to 5T and from 5T to 5.5T respectively. Blue and black plots correspond to the amplitude average for the field sweep from 5.5T to 5T and from 5T to 5.5T.

Overall, excitation current has an impact on the maximum and average amplitude of the AB oscillations.

## 5.5 Behavior near zero magnetic field

During full range measurement of the rings, some remarkable behavior was observed near zero magnetic field. Magnetoresistance of the ring D12 in the field regime -0.5T to 0.5T plotted in Figure 5.17. The excitation current was 30nA and the temperature was ~260mK.

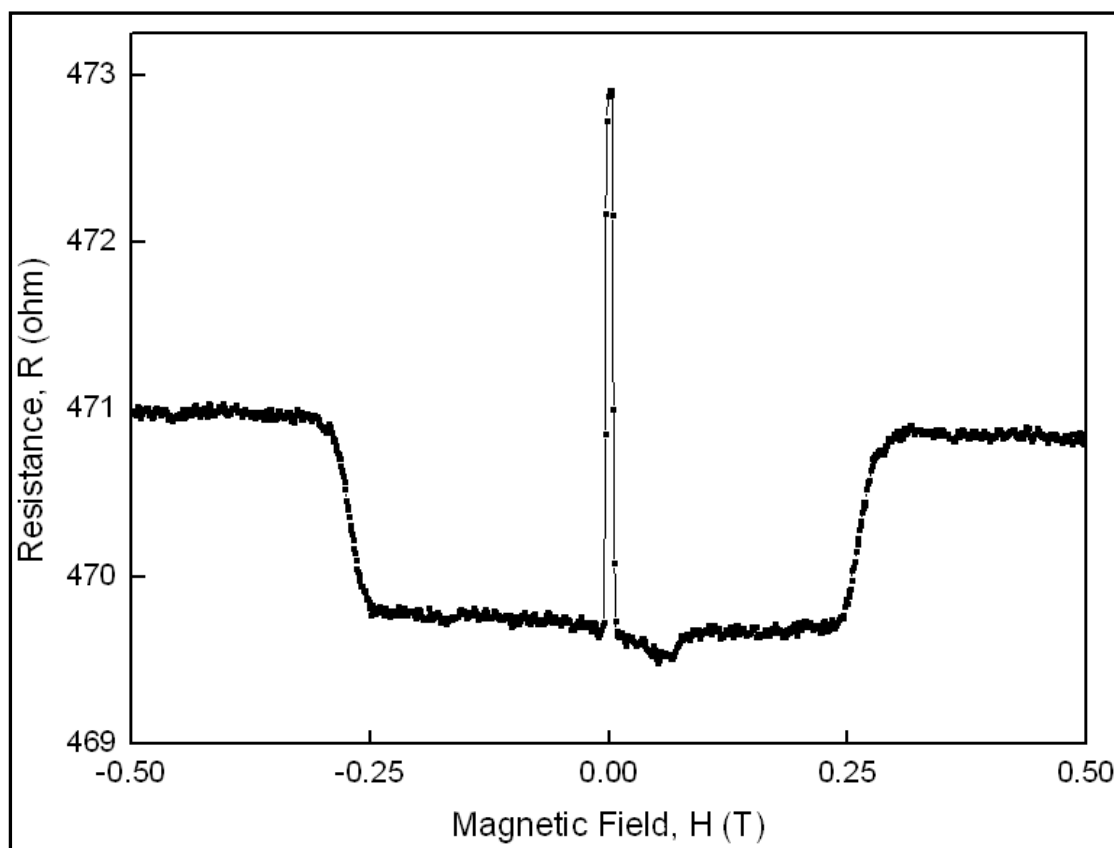


Figure 5.17: Magnetoresistance of ring D12 before subtracting the polynomial fit in the field regime  $-0.5\text{T}$  to  $0.5\text{T}$  with a step size of  $1\text{mT}$ . The excitation current is  $30\text{nA}$  and the temperature is  $\sim 260\text{mK}$ .

Three phenomena can be observed from Figure 5.17 - sharp resistance steps around  $-0.25\text{T}$  and  $0.25\text{T}$ , a sudden increase of the resistance around  $0\text{T}$  and decreasing behavior of the resistance around  $0.1\text{T}$ .

Al bonding wire was suspected for the resistance deep at  $0.25\text{T}$ . It could be that Al bonding wires are superconducting at  $260\text{mK}$  and very low magnetic field. In order to verify this issue, the sample was rebonded with gold bounding wire. The measurement results are shown in section 5.5.1.

To explore the sudden increase of resistance issue, a measurement was taken for a short range of field near zero magnetic field. Magnetic field was swept from  $-0.02\text{T}$  to  $-0.02\text{T}$ , then  $-0.02\text{T}$  to  $0.02\text{T}$  and again  $0.02\text{T}$  to  $-0.02\text{T}$  with a step size of  $1\text{mT}$ . The excitation current was  $30\text{nA}$  and the temperature was  $\sim 260\text{mK}$ . Corresponding results are plotted in Figure 5.18.

It can be said from the Figure 5.18 that these three plots matched with each other. Initially it was assumed that it could be the weak localization peak. But it looks like a jump instead of exponential increase. Moreover, this behavior is not reproducible. However, this behavior remains unexplained.

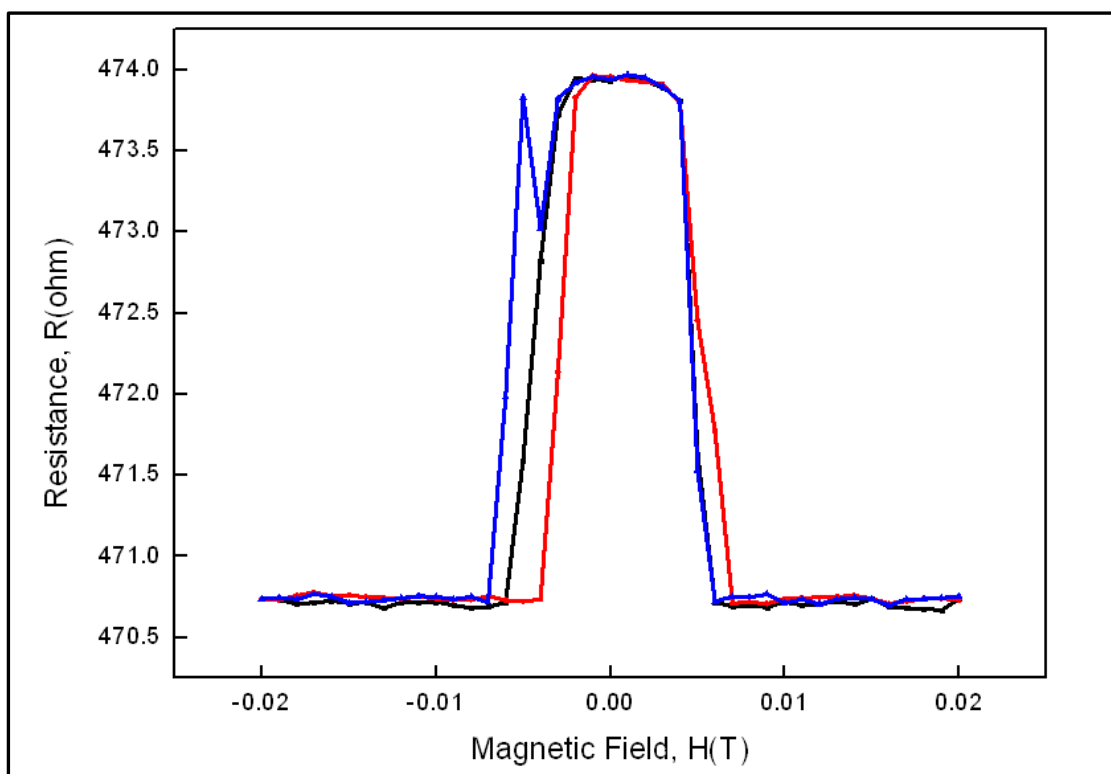


Figure 5.18: Magnetoresistance of ring D12 before subtracting the polynomial fit in the field regime 0.02T to -0.02T (black), -0.02T to 0.02T (red) and 0.02T to -0.02T (blue) with a step size of 1mT. The excitation current is 30nA and the temperature is  $\sim 260$ mK.

To investigate the resistance dip issues, Au wire is used to bond the samples instead of Al wire.

### 5.5.1 AB oscillations for gold wire bonded ring

After taking out the sample from the Heliox, it was wire bonded again using Au wire. In such a way, possible superconducting behavior from the bounding wire is ruled out. At that time only ring H5 was working properly. After cooling down at 250mK, magnetic field was swept from 7T to -7T with a step size of 2mT and full range measurement was taken. The excitation current was 65nA.

It was possible to observe the AB oscillations in different ranges. The best oscillation range was found between 6T to 5.5T and also 9.3mT AB period was observed which is in agreement with the theoretical value and the previous practical experiment (ring H12). The oscillation and FFT are shown in the following Figure 5.19 and 5.20 respectively.

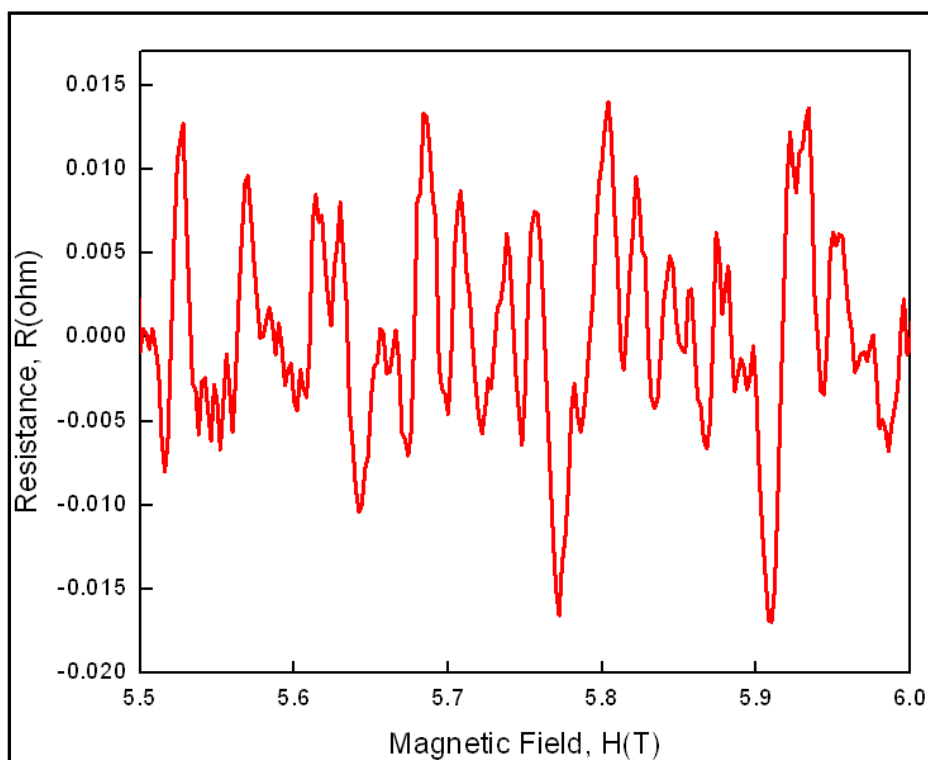


Figure 5.19: Magnetoresistance of ring H5 after subtracting the polynomial fit in the field regime 5.5T to 6T with a step size of 2mT (smoothed for 5 points). The excitation current is 65nA and the temperature is 250mK.

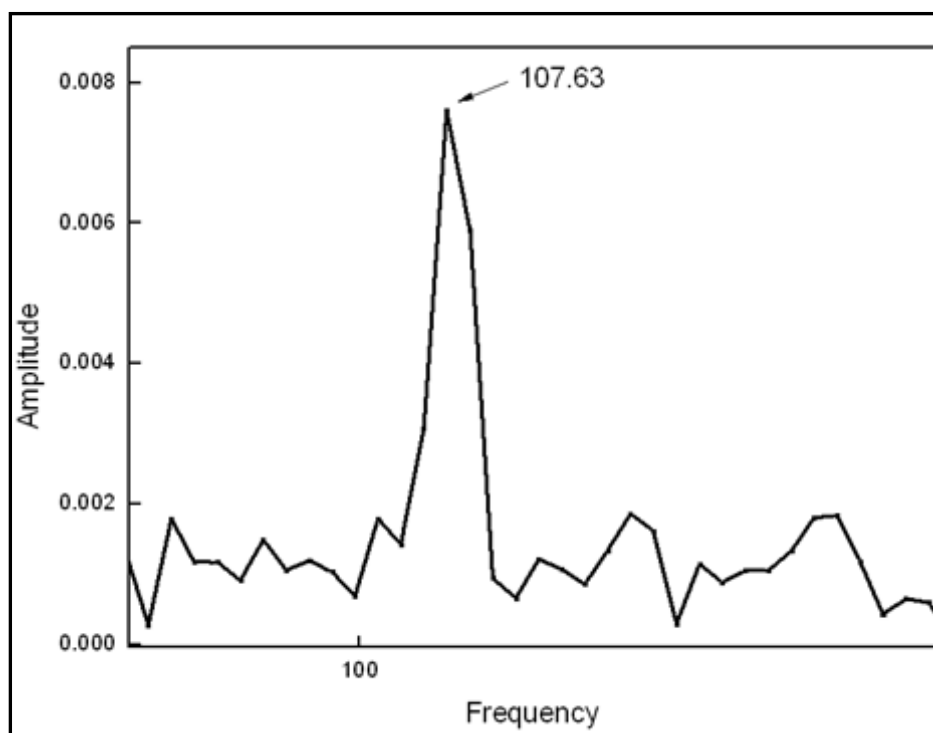


Figure 5.20: FFT for the data presented in Figure 5.19. Peak position is at 107.63.

## 5.5.2 Behavior near Zero Field for gold bonded ring (ring H5)

To investigate the issue near zero field, a close range around zero field was chosen (-1T to 1T). Then a measurement was taken by sweeping the magnetic field in both directions consecutively for three times with a step size of 2mT at 248mK. The excitation current was 65nA. Magnetoconductance for ring H5 are plotted in Figure 5.21.

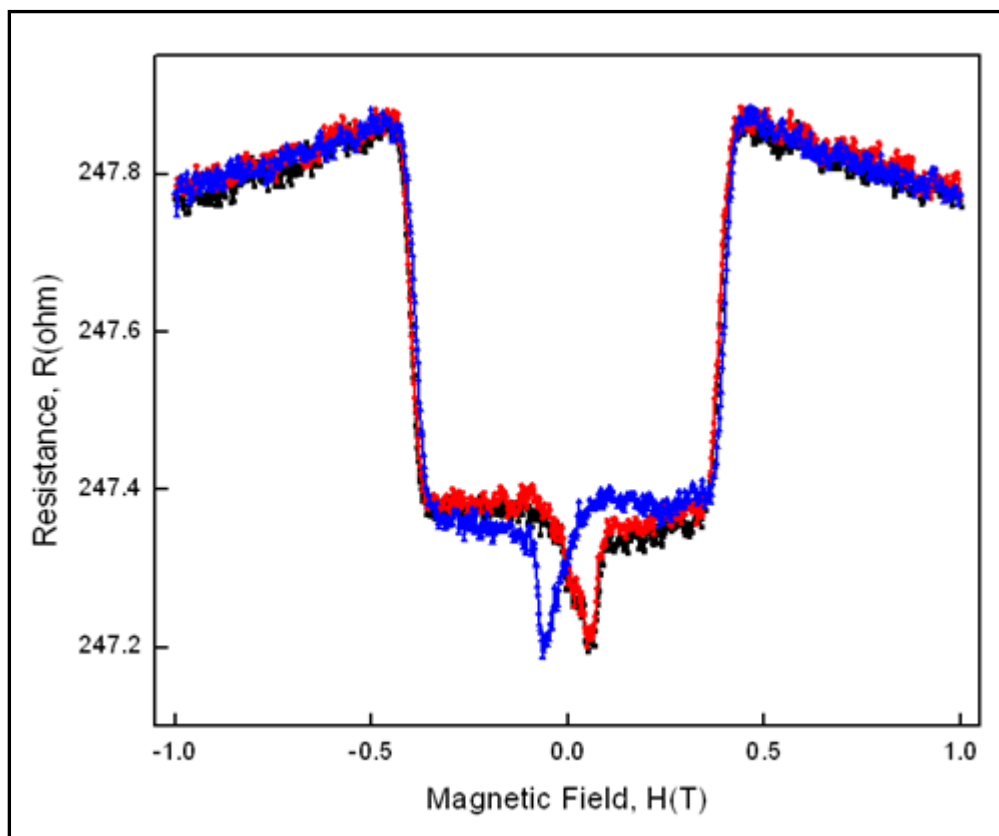


Figure 5.21: Magnetoconductance of ring H5 before subtracting the polynomial fit in the field regime field -1T to 1T (black), 1T to -1T (blue) and -1T to 1T (red) with a step size of 2mT. The excitation current is 65nA and the temperature is 248mK.

At least two of the plots have matched exactly with each other (black and red); the blue plot is also slightly matched with the other two plots. It is still possible to observe the resistance deep at 0.5T. Also decreasing behavior of the resistance is evident from the above Figure 5.21. There is no sudden increase of resistance issue in this case.

The resistance dip can be observed in the ring even after bonded with gold wire. So it can be said that this effect was not generated from Al wire. Generally rings are directly connected with the contact pads and the big bar (line h); schematic diagram of the connection map is plotted in Figure 5.22. To explore the resistance deep case, a measurement was taken on line H in the field regime -1T to 1T and 1T to -1T with a step size of 2mT. The excitation current was 5 $\mu$ A. The results of these measurements are plotted in Figure 5.23.

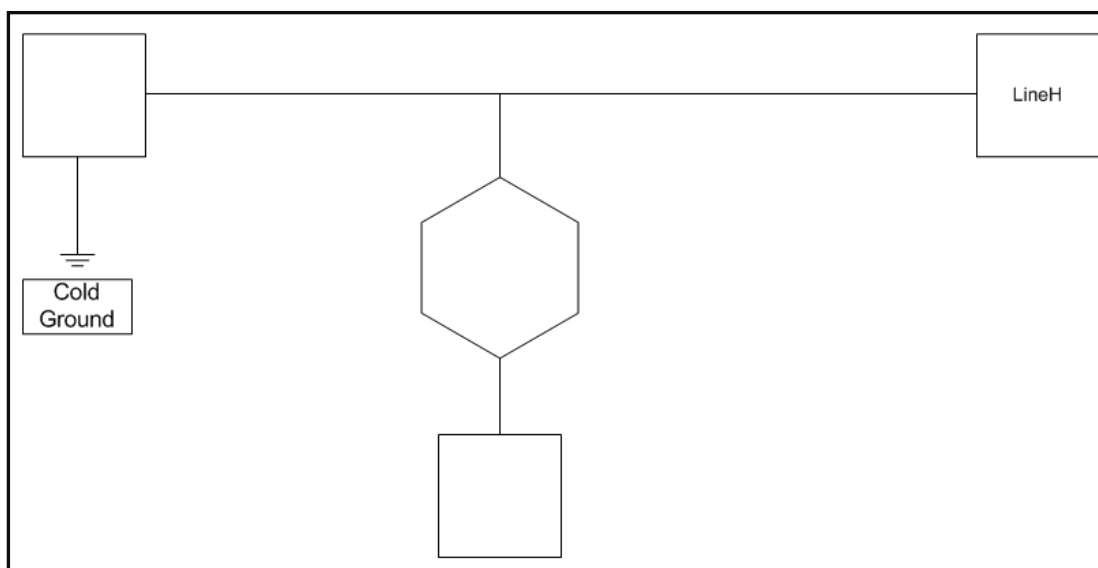


Figure 5.22: Schematic diagram of a ring with corresponding contact pads.

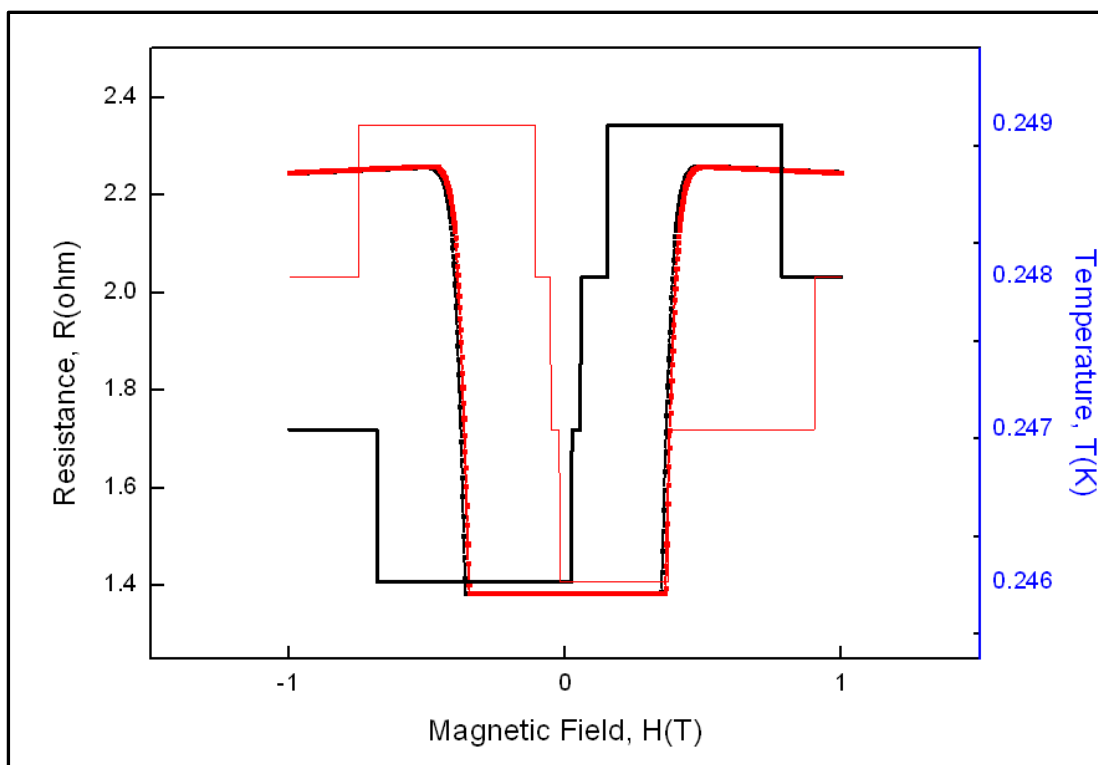


Figure 5.23: Magnetoresistance of Line H in the field regime field -1T to 1T (black dashed line) and 1T to -1T (red dashed line) with a step size of 2mT. The excitation current is  $5\mu\text{A}$ . Solid black and red line corresponds to the temperature sensor of  $^3\text{He}$ .

Comparing Figure 5.21 and Figure 5.23, it can be said that the resistance dip is due to the contact pads connected with the ring. These pads are prepared with 100nm Ti layer and 300nm Au layer. Ti layer is suspected for this superconductive behavior.

To explore the resistance decreasing behavior (which occurred after 0T), resistance was measured at different temperature starting from 245mK till 1.76K. The corresponding results are plotted in Figure 5.24.

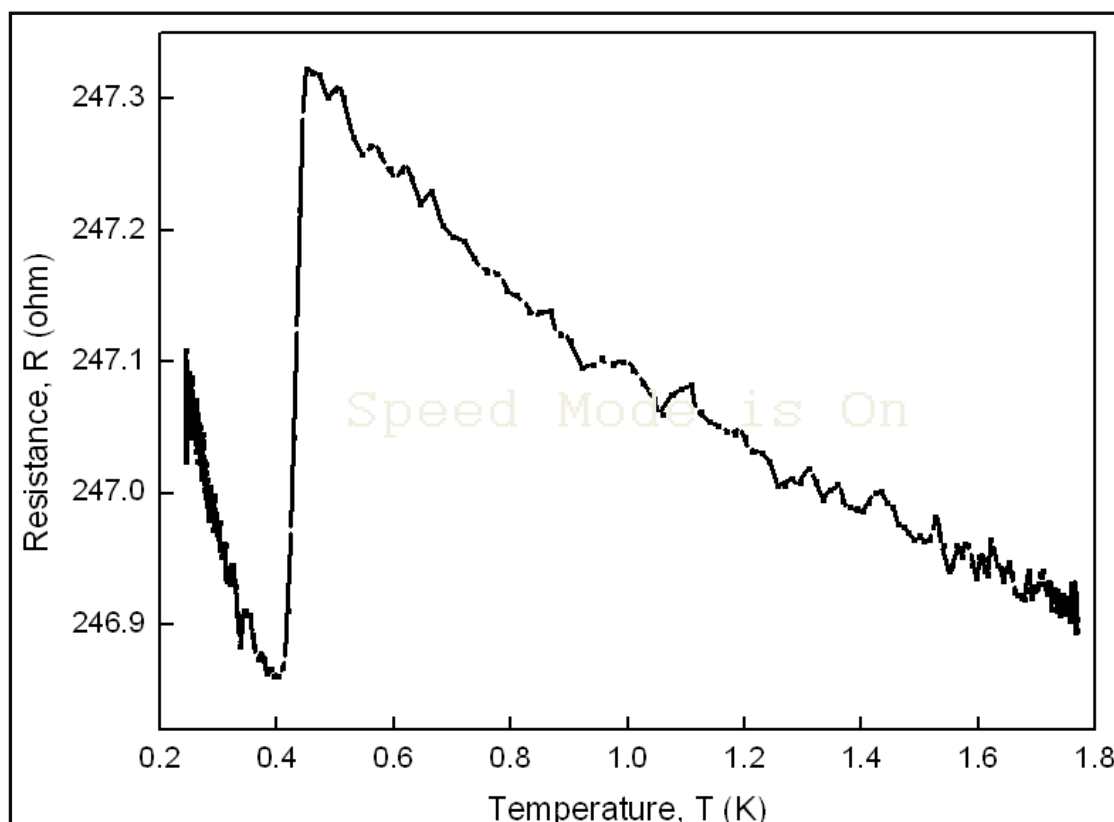
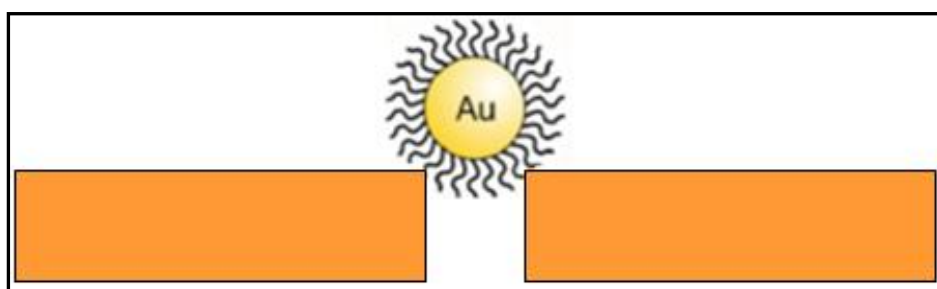


Figure 5.24: Resistance of the ring H5 at different temperature.

Two behaviors can be observed from the above Figure 5.24. First one is superconducting behavior at 0.4K and second one looks like Kondo effect. Around 0.4T, when temperature increases, resistance decreases. The change of temperature can also be observed from the temperature sensor data of Figure 5.23. Temperature increases due to the heating behavior. So heating is responsible for the decreasing resistance near zero field.

# Chapter 6: Conclusions and Recommendations

---



## 6.1 Conclusions

One of the primary goals was to observe the AB oscillation from the rings. To achieve this goal, required modification of the wiring has been performed. Samples were fabricated using e-beam lithography and photolithography. Low temperature measurement had performed to observe the AB oscillations. Following conclusions can be drawn from the experiments.

- AB oscillations were observed for rings with different sizes.
- Comparison of the expected AB periods and the measured AB periods can be found in Table 6.1. The period of the oscillation is in agreement with the calculated value for rings with different dimensions.

Table -6.1: Comparison theoretical and measured value of the AB period

Ring	Theoretical value (mT)	Measured Value (mT)
H12 (bonded with Al wire)	9.2	9.3
D12 (bonded with Al wire)	20.7	20.8
H5 (bonded with Gold wire)	20.2	9.3

- These AB periods were robust for different temperatures and excitation currents.
- Amplitude of the oscillations decreases by increasing temperature or excitation current. Both this behavior is related with the coherence length and the condition that electrons energy needed to be lower than the thermal energy,  $k_B T$ .
- Also a resistance dip has been observed near zero field. It was found that the Ti in the contact pads is responsible for such superconducting behavior.
- Due to insufficient time, it was not possible to insert the NPs in the gap. Otherwise, it would be interesting to see the results of the nanoparticle bridging. Now the next step should be to find the best way to insert the NPs in the gap.

## 6.2 Recommendations

As the main aim is to insert the NPs in one arm of the AB ring, a modification has been made in the design. A new structure has introduced where one arm of the ring has designed as junction with space while the other arm has designed as line with gap. A Clewin design of this new type of structures has shown in Figure 6.1.

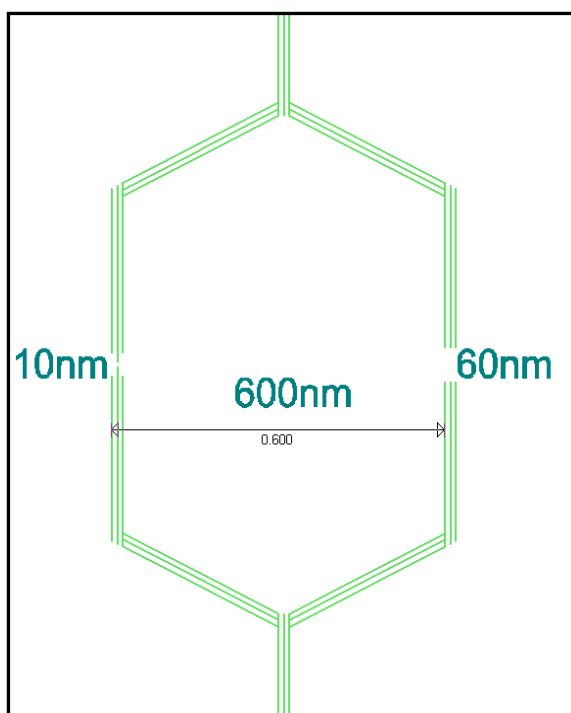


Figure -6.1: Clewin Design of the New Ring R. Width of the ring 600nm, Junction with space size 10nm and line with gap size 60nm

In the modified design, junction with space has designed for higher resistance. It is possible to test the actual junction resistance of the sample. Lines with different gap sizes are made. All of these types of structures are designed together so that later saw can be used to divide the samples. In this way NPs insertion can be tested separately. Also some rings are designed to check the AB oscillation.

As it is not possible to do the EB writing at MESA+, design was sent to delft and a request was made to the collaborator of NanoElectronics Group Mrs. Anja van Langen-Suurling to write the sample. As in Delft, different software (layoutbeamer) has used; that is why it was not possible to see the lines if the line width is zero nanometer (like Japanese Sample). This is why each line needed to defined as 2nm width. A detailed bonding map can be found in Table 6.2

Table – 6.2: Design map of the modified design

	1-4	5-8	9-12	13-16	17-20	21-24	Type of structure	Dimension
A	40	40	60	80	100	120	Line with gap	gap size (nm)
B	40	40	60	80	100	120	Line with gap	gap size (nm)
C	40	40	60	80	100	120	Line with gap	gap size (nm)
D	40	40	60	80	100	120	Line with gap	gap size (nm)
E	60	60	60	60	60	60	Line with gap	gap size (nm)
F	80	80	80	80	80	80	Line with gap	gap size (nm)
G	100	100	100	100	100	100	Line with gap	gap size (nm)
H	120	120	120	120	120	120	Line with gap	gap size (nm)
I	0	0	6	6	8	8	Junction with space	Space size (nm)
J	10	10	10	12	12	12	Junction with space	Space size (nm)
K	0	0	6	6	8	8	Junction with space	Space size (nm)
L	10	10	10	12	12	12	Junction with space	Space size (nm)
M	300	300	300	400	400	400	Ring	gap size (nm)
N	300, 6, 60	300, 6, 60	300, 6, 60	400, 8, 80	400, 8, 80	400, 8, 80	Ring, Junction w space, Line w gap	Width of the ring (nm), Junction, Line
O	500	500	500	500	500	500	Ring	gap size (nm)
P	500, 8, 60	500, 8, 60	500, 8, 60	500, 10, 80	500, 10, 80	500, 10, 80	Ring, Junction w space, Line w gap	Width of the ring (nm), Junction, Line
Q	600	600	600	600	600	600	Ring	gap size (nm)
R	600, 10, 60	600, 10, 60	600, 12, 60	600, 12, 60	600, 12, 60	600, 12, 60	Ring, Junction w space, Line w gap	Width of the ring (nm), Junction, Line



Figure 6.2: SEM results of line with gap structure from Delft

A SEM image of line with structures (test structures) written by written by Mr.s Anja has shown in the Figure 6.2. Expected line width and gap size is 40nm. In both cases, promising results has found.

The samples were already written and ready for photolithography process. It would be easier for the future person to continue the project without waiting for the sample.

The next step would be inserting NPs in the ring arm. From literature study[9], it was seen that if the particle size is bigger than the gap, then it is possible to properly close the gap by one nanoparticle result in the lowest resistance. For both Japanese and Delft sample maximum gap is 80nm, Also there are couple of gaps of 40nm. So for this project, size of the chosen NPs is 100nm. At first, unmodified NPs need to be inserted by applying alternating electric field using Dielectrophoresis technique. Then depending on the results, particles can be modified and inserted in the gap.

# References

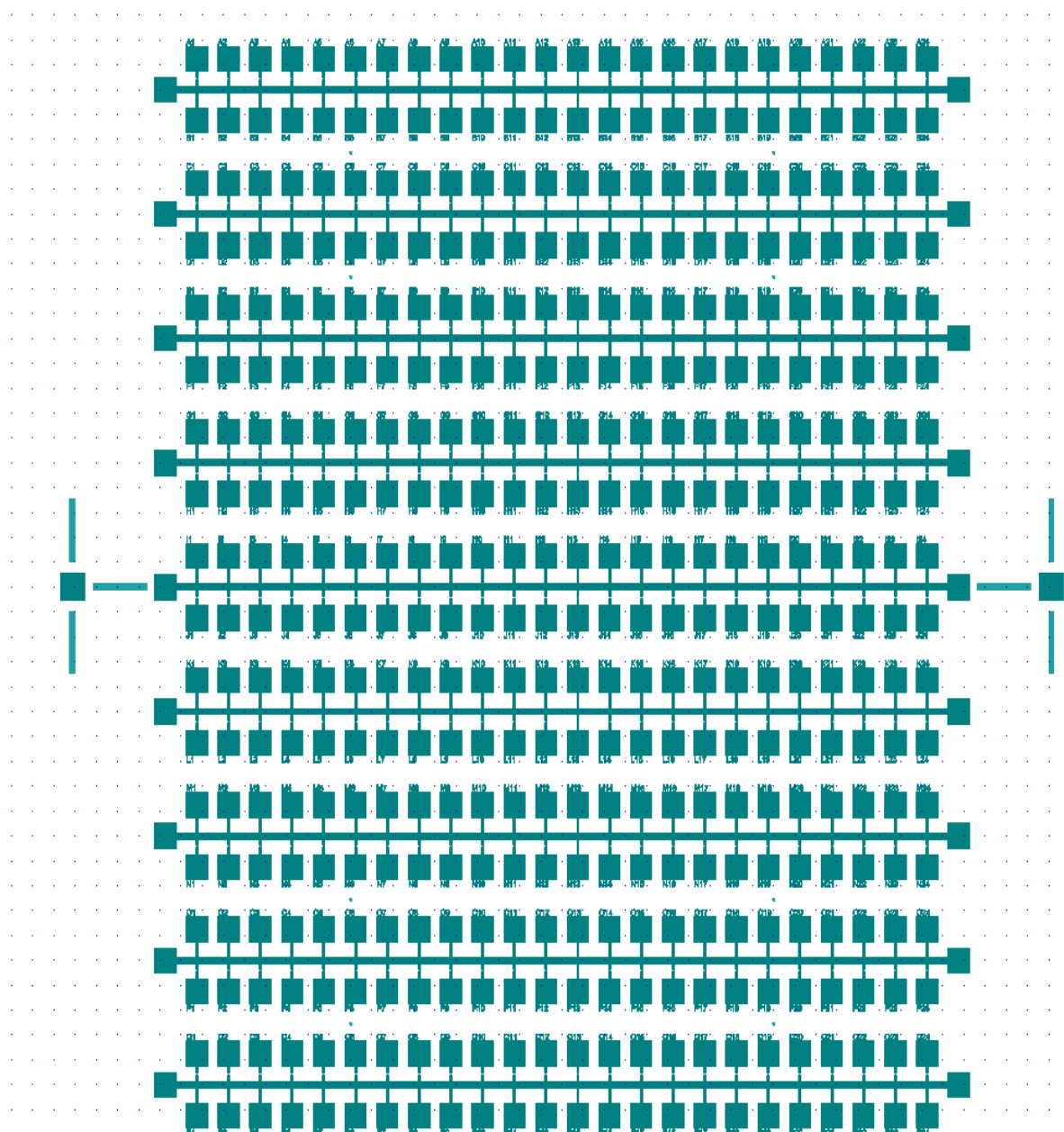
---

1. Moore, G.E., *Cramming more components onto integrated circuits*. Proceedings of the IEEE, 1998. **86**(1): p. 82-85.
2. Groningen, U.o. *Aharonov Bohm* [cited 2010 June 23]; Available from: <http://msc.phys.rug.nl/QuantumMechanics/ab.htm>.
3. Ghassemi, S., *A study of the Coherency of Electron Transport Through Organic Molecules using Aharonov-Bohm Interferometer*, in *Nanoelectronics 2009*, University of Twente: Enschede p. 104.
4. Webb, R.A., et al., *Observation of  $h/e$  Aharonov-Bohm Oscillations in Normal- Metal Rings*. Physical Review Letters 1985. **54**(25): p. 4.
5. Aharonov, Y. and D. Bohm, *Significance of electromagnetic potentials in the quantum theory*. Physical Review, 1959. **115**(3): p. 485-491.
6. Lee, P.A. and A.D. Stone, *Universal Conductance Fluctuations in Metals*. Physical Review Letters, 1985. **55**(15): p. 1622.
7. Aihara, K., et al., *Temperature dependence of the phase coherence length of high-mobility AlGaAs/GaAs quantum-wire rings*. Japanese Journal of Applied Physics, Part 1: Regular Papers and Short Notes and Review Papers, 1991. **30**(9 B): p. 1627-1630.
8. Dumpich, G. and A. Carl, *Anomalous temperature dependence of the phase-coherence length for inhomogeneous gold films*. Physical Review B, 1991. **43**(14): p. 12074-12077.
9. Amlani, I., et al., *An approach to transport measurements of electronic molecules*. Applied Physics Letters, 2002. **80**(15): p. 2761-2763.
10. Instruments, O., *Heliox VL Manual and Data*.

# Appendices

---

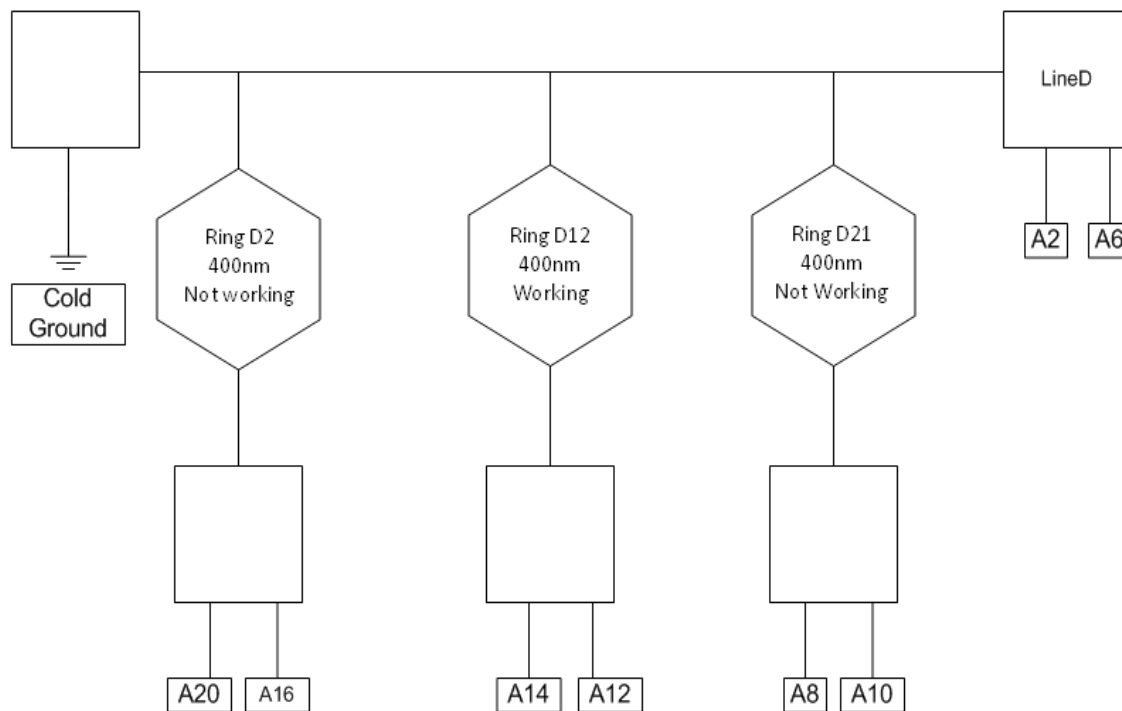
## Appendix 1 Mask Layout for contact pads



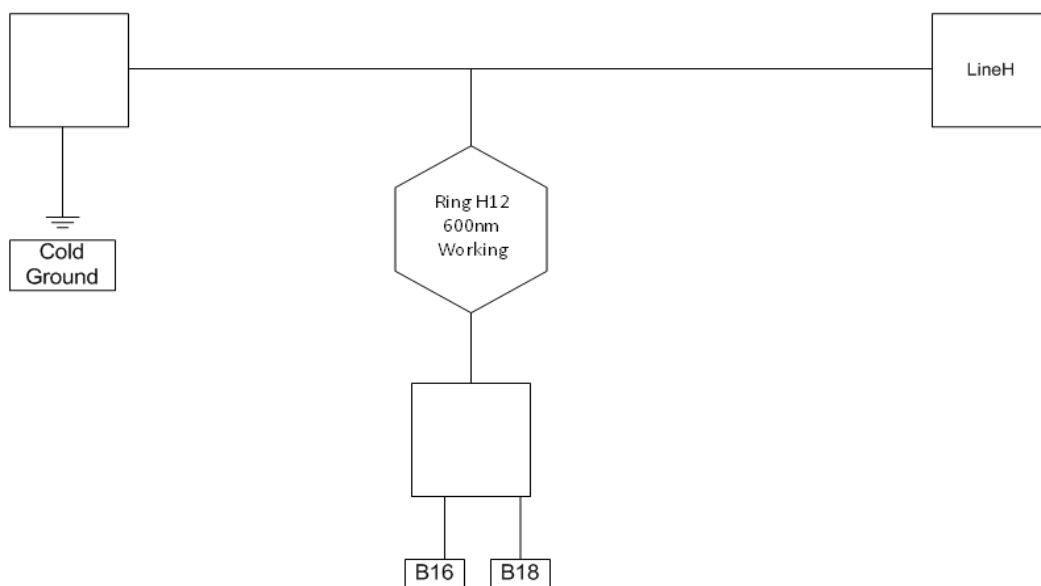
## Appendix 2 Connection Diagram

Only current source and voltage source connections are shown.

### Appendix 2.1 Connection diagram for Ring D bonded with Al wire

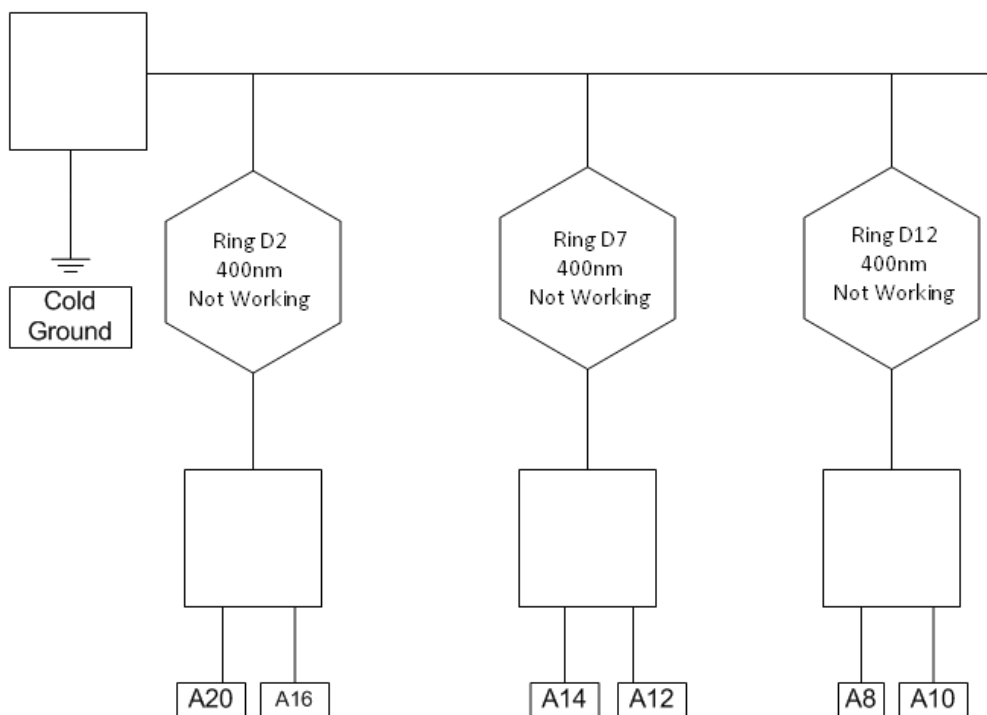


### Appendix 2.2 Connection diagram for Ring H bonded with Al wire



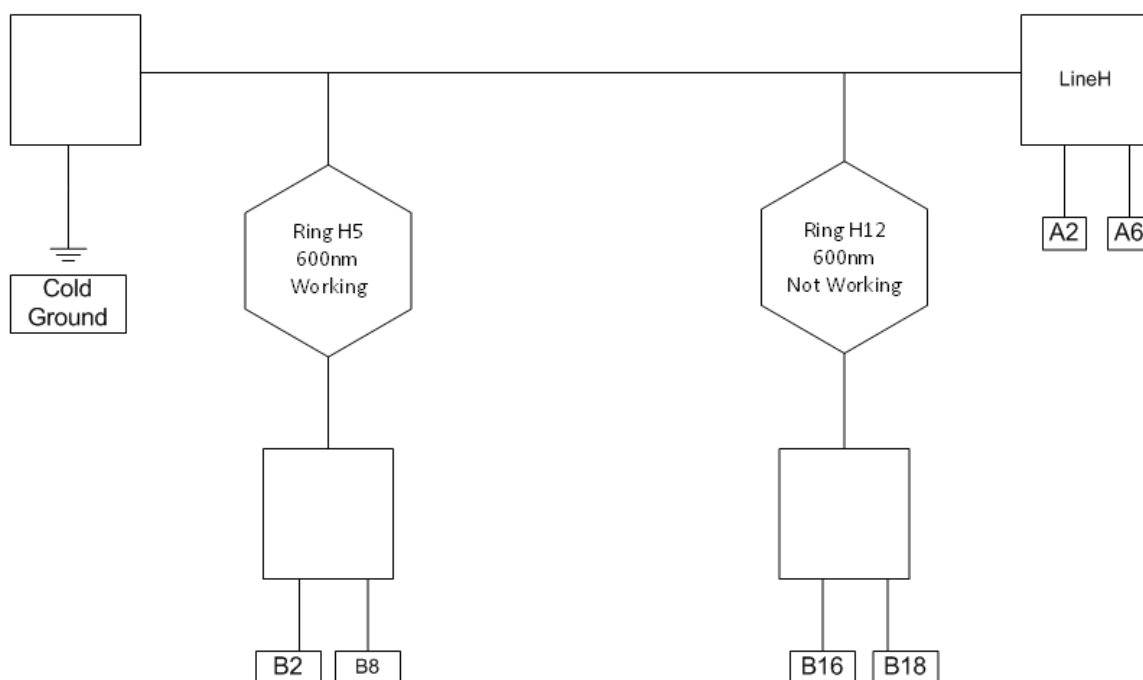
### Appendix 2.3 Wire

### Connection Diagram for Ring H bonded with Au



### Appendix 2.4 Wire

### Connection Diagram for Ring H bonded with Au



### Appendix 3 Calculation of AB Period of a ring

To calculate the AB period, we first need to calculate the area of hexagonal ring. As it's not a regular hexagon, we divided our hexagon as triangle and rectangle. Then from the design file we take the corresponding value,

*Area of the Hexagon = 2 × Area of the triangle + Area of the Rectangle*

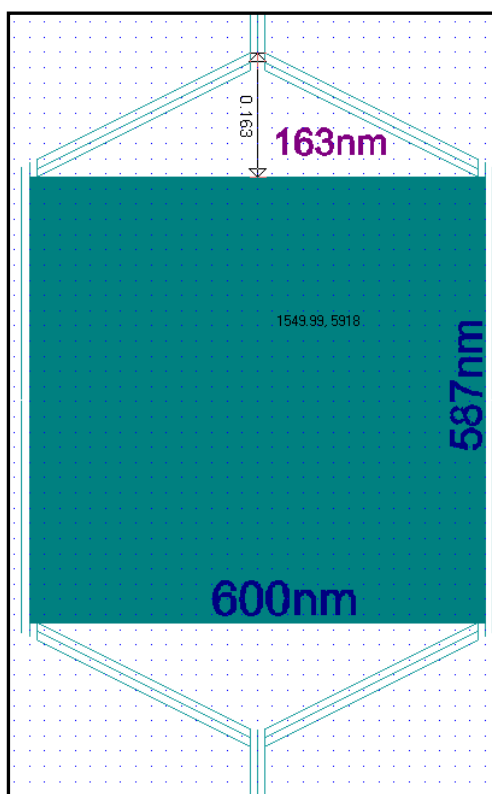
$$AB \text{ Period, } \Delta B = \frac{h}{eS}$$

*Here,  $h$  = Planck's Constant =  $6.626068 \times 10^{-34} \text{ m}^2 \text{ kg/s}$*

*$e$  = electrons charge =  $1.602 \times 10^{-19} \text{ C}$*

*$S$  = Area of the Hexagon*

For an example, for Ring H (600nm), we took the corresponding value from the Clewin design file



From the above figure,

$$\text{Area of the triangle} = \frac{1}{2} \times 600\text{nm} \times 163\text{nm} = 4.89 \times 10^{-14} \text{ m}^2$$

$$\text{Area of the rectangle} = 600\text{nm} \times 587\text{nm} = 3.522 \times 10^{-13} \text{ m}^2$$

$$\begin{aligned} \text{Area of the Ring H(600nm)} &= (2 \times 4.894.89 \times 10^{-14}) + 3.522 \times 10^{-13} \\ &= 4.5 \times 10^{-13} \text{ m}^2 \end{aligned}$$

$$\text{Now the AB period } \Delta B = \frac{h}{eS} = \frac{6.626068 \times 10^{-34}}{1.602 \times 10^{-19} \times 4.5 \times 10^{-13}} = 9.2 \text{ mT}$$

We calculated the AB period for other rings in the above way.

## Appendix 4 Measurement parameters for different rings

All the measurement parameters for different experiments are listed in this appendix. Red color indicates the changed value for different experiment.

### Appendix 4.1 Measurement Parameters for Ring H12

Parameters	Value	Parameters	Value	Parameters	Value
Field Range	-5T to 5T	Sweep Rate	0.1T/min	Amplitude	0.300V
Step size	2mT	X noise	0.03 mV	Frequency	179.13 Hz
Time Constant	1s	Y noise	0.03 mV	Temperature	258mK
Sensitivity	200mV	Offset	78% (expand 10 times)		

Parameters	Value	Parameters	Value	Parameters	Value
Field Range	-7T to +7T	Sweep Rate	0.1T/min	Amplitude	0.300
Step size	2mT	X noise	0.03 mV	Frequency	179.13 Hz
Time Constant	1s	Y noise	0.03 mV	Temperature	258mK
Sensitivity	200mV	Offset	78% (expand 10 times)		

### Temperature Dependence

Parameters	Value	Parameters	Value	Parameters	Value
Field Range	-1.7T to 1.2T	Sweep Rate		Amplitude	0.300V
Step size	0.4mT	X noise	0.03 mV	Frequency	179.13 Hz
Time Constant	1s	Y noise	0.03 mV	Temperature	261mK
Sensitivity	200mV	Offset	78% (expand 10 times)		

Parameters	Value	Parameters	Value	Parameters	Value
Field Range	-1.2T to -1.7T	Sweep Rate	0.1T/min	Amplitude	0.300V
Step size	0.4mT	X noise	0.03 mV	Frequency	179.13 Hz
Time Constant	1s	Y noise	0.03 mV	Temperature	261mK
Sensitivity	200mV	Offset	78% (expand 10 times)		

Parameters	Value	Parameters	Value	Parameters	Value
Field Range	-1.7T to -1.2T	Sweep Rate	0.1T/min	Amplitude	0.300V
Step size	0.4mT	X noise	0.03 mV	Frequency	179.13 Hz
Time Constant	1s	Y noise	0.02 mV	Temperature	300mK
Sensitivity	200mV	Offset	78% (expand 10 times)		

Parameters	Value	Parameters	Value	Parameters	Value
Field Range	-1.2T to -1.7T	Sweep Rate	0.1T/min	Amplitude	0.300V
Step size	0.4mT	X noise	0.03 mV	Frequency	179.13 Hz
Time Constant	1s	Y noise	0.02 mV	Temperature	300mK
Sensitivity	200mV	Offset	78% (expand 10 times)		

Parameters	Value	Parameters	Value	Parameters	Value
Field Range	-1.7T to -1.2T	Sweep Rate	0.1T/min	Amplitude	0.300V
Step size	0.4mT	X noise	0.02 mV	Frequency	179.13 Hz
Time Constant	1s	Y noise	0.03 mV	Temperature	350mK
Sensitivity	200mV	Offset	78% (expand 10 times)		

Parameters	Value	Parameters	Value	Parameters	Value
Field Range	-1.2T to -1.7T	Sweep Rate	0.1T/min	Amplitude	0.300V
Step size	0.4mT	X noise	0.02 mV	Frequency	179.13 Hz
Time Constant	1s	Y noise	0.03 mV	Temperature	350mK
Sensitivity	200mV	Offset	78% (expand 10 times)		

Parameters	Value	Parameters	Value	Parameters	Value
Field Range	-1.7T to -1.2T	Sweep Rate	0.1T/min	Amplitude	0.300V
Step size	0.4mT	X noise	0.03 mV	Frequency	179.13 Hz
Time Constant	1s	Y noise	0.03 mV	Temperature	400mK
Sensitivity	200mV	Offset	78% (expand 10 times)		

Parameters	Value	Parameters	Value	Parameters	Value
Field Range	-1.2T to -1.7T	Sweep Rate	0.1T/min	Amplitude	0.300V
Step size	0.4mT	X noise	0.03 mV	Frequency	179.13 Hz
Time Constant	1s	Y noise	0.03 mV	Temperature	400mK
Sensitivity	200mV	Offset	78% (expand 10 times)		

Parameters	Value	Parameters	Value	Parameters	Value
Field Range	-1.7T to -1.2T	Sweep Rate	0.1T/min	Amplitude	0.300V
Step size	0.4mT	X noise	0.03 mV	Frequency	179.13 Hz
Time Constant	1s	Y noise	0.03mV	Temperature	500mK
Sensitivity	200mV	Offset	78% (expand 10 times)		
Parameters	Value	Parameters	Value	Parameters	Value
Field Range	-1.2T to -1.7T	Sweep Rate	0.1T/min	Amplitude	0.300V
Step size	0.4mT	X noise	0.03 mV	Frequency	179.13 Hz
Time Constant	1s	Y noise	0.03 mV	Temperature	500mK
Sensitivity	200mV	Offset	78% (expand 10 times)		

### Excitation Current Dependence

Parameters	Value	Parameters	Value	Parameters	Value
Field Range	-1.7T to -1.2T	Sweep Rate	0.1T/min	Amplitude	0.100V
Step size	0.4mT	X noise	0.03 mV	Frequency	179.13 Hz
Time Constant	1s	Y noise	0.0 3mV	Temperature	261mK
Sensitivity	100mV	Offset	49% (expand 10 times)		

Parameters	Value	Parameters	Value	Parameters	Value
Field Range	-1.2T to -1.7T	Sweep Rate	0.1T/min	Amplitude	0.100V
Step size	0.4mT	X noise	0.03 mV	Frequency	179.13 Hz
Time Constant	1s	Y noise	0.03 mV	Temperature	261mK
Sensitivity	100mV	Offset	49% (expand 10 times)		
Parameters	Value	Parameters	Value	Parameters	Value
Field Range	-1.7T to -1.2T	Sweep Rate	0.1T/min	Amplitude	0.200V
Step size	0.4mT	X noise	0.03mV	Frequency	179.13 Hz
Time Constant	1s	Y noise	0.03 mV	Temperature	261mK
Sensitivity	200mV	Offset	49% (expand 10 times)		
Parameters	Value	Parameters	Value	Parameters	Value
Field Range	1.2T to -1.7T	Sweep Rate	0.1T/min	Amplitude	0.200V
Step size	0.4mT	X noise	0.03 mV	Frequency	179.13 Hz
Time Constant	1s	Y noise	0.03 mV	Temperature	261mK
Sensitivity	200mV	Offset	49% (expand 10 times)		

Parameters	Value	Parameters	Value	Parameters	Value
Field Range	-1.7T to -1.2T	Sweep Rate	0.1T/min	Amplitude	0.300V
Step size	0.4mT	X noise	0.00 mV	Frequency	179.13 Hz
Time Constant	1s	Y noise	0.00 mV	Temperature	262mK
Sensitivity	200mV	Offset	78% (expand 10 times)		

Parameters	Value	Parameters	Value	Parameters	Value
Field Range	1.2T to -1.7T	Sweep Rate	0.1T/min	Amplitude	0.300V
Step size	0.4mT	X noise	0.00 mV	Frequency	179.13 Hz
Time Constant	1s	Y noise	0.00mV	Temperature	262mK
Sensitivity	200mV	Offset	78% (expand 10 times)		

Parameters	Value	Parameters	Value	Parameters	Value
Field Range	-1.7T to -1.2T	Sweep Rate	0.1T/min	Amplitude	0.350V
Step size	0.4mT	X noise	0.02 mV	Frequency	179.13 Hz
Time Constant	1s	Y noise	0.03 mV	Temperature	262mK
Sensitivity	200mV	Offset	92% (expand 10 times)		

Parameters	Value	Parameters	Value	Parameters	Value
Field Range	1.2T to -1.7T	Sweep Rate	0.1T/min	Amplitude	0.350V
Step size	0.4mT	X noise	0.02 mV	Frequency	179.13 Hz
Time Constant	1s	Y noise	0.03 mV	Temperature	262mK
Sensitivity	200mV	Offset	92% (expand 10 times)		

### Appendix 4.2 Measurement Parameters for Ring D12

Parameters	Value	Parameters	Value	Parameters	Value
Field Range	-7T to 7T	Sweep Rate	0.1T/min	Amplitude	0.300V
Step size	1mT	X noise	0.03 mV	Frequency	179.13 Hz
Time Constant	1s	Y noise	0.02 mV	Temperature	261mK
Sensitivity	500mV	Offset	49% (expand 10 times)		

Parameters	Value	Parameters	Value	Parameters	Value
Field Range	7T to -7T	Sweep Rate	0.1T/min	Amplitude	0.300V
Step size	1mT	X noise	0.03 mV	Frequency	179.13 Hz
Time Constant	1s	Y noise	0.02 mV	Temperature	261mK
Sensitivity	500mV	Offset	49% (expand 10 times)		

### Temperature Dependence

Parameters	Value	Parameters	Value	Parameters	Value
Field Range	5.5T to 5T	Sweep Rate	0.1T/min	Amplitude	0.300V
Step size	1mT	X noise	0.03 mV	Frequency	179.13 Hz
Time Constant	1s	Y noise	0.03 mV	Temperature	261mK
Sensitivity	500mV	Offset	49% (expand 10 times)		

Parameters	Value	Parameters	Value	Parameters	Value
Field Range	5T to 5.5T	Sweep Rate	0.1T/min	Amplitude	0.300V
Step size	1mT	X noise	0.03 mV	Frequency	179.13 Hz
Time Constant	1s	Y noise	0.03 mV	Temperature	261mK
Sensitivity	500mV	Offset	49% (expand 10 times)		

Parameters	Value	Parameters	Value	Parameters	Value
Field Range	5.5T to 5T	Sweep Rate	0.1T/min	Amplitude	0.300V
Step size	1mT	X noise	0.00 mV	Frequency	179.13 Hz
Time Constant	1s	Y noise	0.00 mV	Temperature	300mK
Sensitivity	500mV	Offset	49% (expand 10 times)		

Parameters	Value	Parameters	Value	Parameters	Value
Field Range	5T to 5.5T	Sweep Rate	0.1T/min	Amplitude	0.300V
Step size	1mT	X noise	0.00 mV	Frequency	179.13 Hz
Time Constant	1s	Y noise	0.00 mV	Temperature	300mK
Sensitivity	500mV	Offset	49% (expand 10 times)		

Parameters	Value	Parameters	Value	Parameters	Value
Field Range	5.5T to 5T	Sweep Rate	0.1T/min	Amplitude	0.300V
Step size	1mT	X noise	0.00 mV	Frequency	179.13 Hz
Time Constant	1s	Y noise	0.00 mV	Temperature	350mK
Sensitivity	500mV	Offset	49% (expand 10 times)		

Parameters	Value	Parameters	Value	Parameters	Value
Field Range	5T to 5.5T	Sweep Rate	0.1T/min	Amplitude	0.300V
Step size	1mT	X noise	0.00 mV	Frequency	179.13 Hz
Time Constant	1s	Y noise	0.00 mV	Temperature	350mK
Sensitivity	500mV	Offset	49% (expand 10 times)		

Parameters	Value	Parameters	Value	Parameters	Value
Field Range	5.5T to 5T	Sweep Rate	0.1T/min	Amplitude	0.300V
Step size	1mT	X noise	0.03 mV	Frequency	179.13 Hz
Time Constant	1s	Y noise	0.03 mV	Temperature	400mK
Sensitivity	500mV	Offset	49% (expand 10 times)		

Parameters	Value	Parameters	Value	Parameters	Value
Field Range	5T to 5.5T	Sweep Rate	0.1T/min	Amplitude	0.300V
Step size	1mT	X noise	0.03 mV	Frequency	179.13 Hz
Time Constant	1s	Y noise	0.03 mV	Temperature	400mK
Sensitivity	500mV	Offset	49% (expand 10 times)		

Parameters	Value	Parameters	Value	Parameters	Value
Field Range	5.5T to 5T	Sweep Rate	0.1T/min	Amplitude	0.300V
Step size	1mT	X noise	0.03 mV	Frequency	179.13 Hz
Time Constant	1s	Y noise	0.03 mV	Temperature	450mK
Sensitivity	500mV	Offset	49% (expand 10 times)		

Parameters	Value	Parameters	Value	Parameters	Value
Field Range	5T to 5.5T	Sweep Rate	0.1T/min	Amplitude	0.300V
Step size	1mT	X noise	0.03 mV	Frequency	179.13 Hz
Time Constant	1s	Y noise	0.03 mV	Temperature	450mK
Sensitivity	500mV	Offset	49% (expand 10 times)		

### Excitation Current Dependence

Parameters	Value	Parameters	Value	Parameters	Value
Field Range	5.5T to 5T	Sweep Rate	0.1T/min	Amplitude	0.100V
Step size	1mT	X noise	0.03 mV	Frequency	179.13 Hz
Time Constant	1s	Y noise	0.03 mV	Temperature	261mK
Sensitivity	500mV	Offset	11% (expand 10 times)	Lock in Gain	0.001

Parameters	Value	Parameters	Value	Parameters	Value
Field Range	5T to 5.5T	Sweep Rate	0.1T/min	Amplitude	0.100V
Step size	1mT	X noise	0.03 mV	Frequency	179.13 Hz
Time Constant	1s	Y noise	0.03 mV	Temperature	261mK
Sensitivity	500mV	Offset	11% (expand 10 times)		

Parameters	Value	Parameters	Value	Parameters	Value
Field Range	5.5T to 5T	Sweep Rate	0.1T/min	Amplitude	0.200V
Step size	1mT	X noise	0.03 mV	Frequency	179.13 Hz
Time Constant	1s	Y noise	0.00 mV	Temperature	261mK
Sensitivity	500mV	Offset	30% (expand 10 times)		

Field Range	5T to 5.5T	Sweep Rate	0.1T/min	Amplitude	0.200V
Step size	1mT	X noise	0.03 mV	Frequency	179.13 Hz
Time Constant	1s	Y noise	0.00 mV	Temperature	261mK
Sensitivity	500mV	Offset	30% (expand 10 times)		

Parameters	Value	Parameters	Value	Parameters	Value
Field Range	5.5T to 5T	Sweep Rate	0.1T/min	Amplitude	0.300V
Step size	1mT	X noise	0.03 mV	Frequency	179.13 Hz
Time Constant	1s	Y noise	0.03 mV	Temperature	261mK
Sensitivity	500mV	Offset	49% (expand 10 times)		

Parameters	Value	Parameters	Value	Parameters	Value
Field Range	5T to 5.5T	Sweep Rate	0.1T/min	Amplitude	0.300V
Step size	1mT	X noise	0.03 mV	Frequency	179.13 Hz
Time Constant	1s	Y noise	0.03 mV	Temperature	261mK
Sensitivity	500mV	Offset	49% (expand 10 times)		

Parameters	Value	Parameters	Value	Parameters	Value
Field Range	5.5T to 5T	Sweep Rate	0.1T/min	Amplitude	0.350V
Step size	1mT	X noise	0.00 mV	Frequency	179.13 Hz
Time Constant	1s	Y noise	0.00 mV	Temperature	261mK
Sensitivity	500mV	Offset	58% (expand 10 times)		

Parameters	Value	Parameters	Value	Parameters	Value
Field Range	5T to 5.5T	Sweep Rate	0.1T/min	Amplitude	0.350V
Step size	1mT	X noise	0.00 mV	Frequency	179.13 Hz
Time Constant	1s	Y noise	0.00 mV	Temperature	261mK
Sensitivity	500mV	Offset	58% (expand 10 times)		

Parameters	Value	Parameters	Value	Parameters	Value
Field Range	5.5T to 5T	Sweep Rate	0.1T/min	Amplitude	0.400V
Step size	1mT	X noise	0.00 mV	Frequency	179.13 Hz
Time Constant	1s	Y noise	0.00 mV	Temperature	261mK
Sensitivity	500mV	Offset	68% (expand 10 times)		

Parameters	Value	Parameters	Value	Parameters	Value
Field Range	5T to 5.5T	Sweep Rate	0.1T/min	Amplitude	0.400V
Step size	1mT	X noise	0.03 mV	Frequency	179.13 Hz
Time Constant	1s	Y noise	0.03 mV	Temperature	261mK
Sensitivity	500mV	Offset	68% (expand 10 times)		

### Near Zero Field case

Parameters	Value	Parameters	Value	Parameters	Value
Field Range	0.02T to -0.02T	Sweep Rate	0.1T/min	Amplitude	0.300V
Step size	1mT	X noise	0.00 mV	Frequency	179.13 Hz
Time Constant	1s	Y noise	0.00 mV	Temperature	260mK
Sensitivity	500mV	Offset	49% (expand 10 times)		

Parameters	Value	Parameters	Value	Parameters	Value
Field Range	-0.02T to 0.02T	Sweep Rate	0.1T/min	Amplitude	0.300V
Step size	1mT	X noise	0.03 mV	Frequency	179.13 Hz
Time Constant	1s	Y noise	0.03 mV	Temperature	260mK
Sensitivity	500mV	Offset	49% (expand 10 times)		

Parameters	Value	Parameters	Value	Parameters	Value
Field Range	0.02T to -0.02T	Sweep Rate	0.1T/min	Amplitude	0.300V
Step size	1mT	X noise	0.00 mV	Frequency	179.13 Hz
Time Constant	1s	Y noise	0.00 mV	Temperature	260mK
Sensitivity	500mV	Offset	49% (expand 10 times)		

### Appendix 4.3 Measurement Parameters for Ring H5 (Bonded with Gold wire)

Parameters	Value	Parameters	Value	Parameters	Value
Field Range	-7T to 7T	Sweep Rate	0.1T/min	Amplitude	0.650V
Step size	2mT	X noise	0.03 mV	Frequency	179.13 Hz
Time Constant	1s	Y noise	0.00 mV	Temperature	252mK
Sensitivity	500mV	Offset	57% (expand 10 times)		

Parameters	Value	Parameters	Value	Parameters	Value
Field Range	7T to -7T	Sweep Rate	0.1T/min	Amplitude	0.650V
Step size	2mT	X noise	0.00 mV	Frequency	179.13 Hz
Time Constant	1s	Y noise	0.00 mV	Temperature	251mK
Sensitivity	500mV	Offset	57% (expand 10 times)		

### Excitation Current Dependence

Parameters	Value	Parameters	Value	Parameters	Value
Field Range	6T to 5.5T	Sweep Rate	0.1T/min	Amplitude	0.650V
Step size	2mT	X noise	0.00 mV	Frequency	179.13 Hz
Time Constant	1s	Y noise	0.00 mV	Temperature	250mK
Sensitivity	500mV	Offset	57% (expand 10 times)		

Parameters	Value	Parameters	Value	Parameters	Value
Field Range	6T to 5.5T	Sweep Rate	0.1T/min	Amplitude	0.700V
Step size	2mT	X noise	0.02 mV	Frequency	179.13 Hz
Time Constant	1s	Y noise	0.03 mV	Temperature	250mK
Sensitivity	500mV	Offset	62% (expand 10 times)		

Parameters	Value	Parameters	Value	Parameters	Value
Field Range	6T to 5.5T	Sweep Rate	0.1T/min	Amplitude	0.750V
Step size	2mT	X noise	0.00mV	Frequency	179.13 Hz
Time Constant	1s	Y noise	0.00 mV	Temperature	250mK
Sensitivity	500mV	Offset	62% (expand 10 times)		

Parameters	Value	Parameters	Value	Parameters	Value
Field Range	5.5T to 6T	Sweep Rate	0.1T/min	Amplitude	0.800V
Step size	2mT	X noise	0.02 mV	Frequency	179.13 Hz
Time Constant	1s	Y noise	0.03 mV	Temperature	252mK
Sensitivity	500mV	Offset	62% (expand 10 times)		

### Near Zero Field case

Parameters	Value	Parameters	Value	Parameters	Value
Field Range	-1T to 1T	Sweep Rate	0.1T/min	Amplitude	0.650V
Step size	2mT	X noise	0.00 mV	Frequency	179.13 Hz
Time Constant	1s	Y noise	0.00 mV	Temperature	249mK
Sensitivity	500mV	Offset	57% (expand 10 times)		

Parameters	Value	Parameters	Value	Parameters	Value
Field Range	1T to -1T	Sweep Rate	0.1T/min	Amplitude	0.650V
Step size	2mT	X noise	0.00 mV	Frequency	179.13 Hz
Time Constant	1s	Y noise	0.00 mV	Temperature	248mK
Sensitivity	500mV	Offset	57% (expand 10 times)		

Parameters	Value	Parameters	Value	Parameters	Value
Field Range	-1T to 1T	Sweep Rate	0.1T/min	Amplitude	0.650V
Step size	2mT	X noise	0.00 mV	Frequency	179.13 Hz
Time Constant	1s	Y noise	0.00 mV	Temperature	248mK
Sensitivity	500mV	Offset	57% (expand 10 times)		